Arabian Journal of Chemistry (2020) 13, 932–953

King Saud University

Arabian Journal of Chemistry

www.ksu.edu.sa
www.sciencedirect.com

ORIGINAL ARTICLE

A detailed experimental and computational study of monocarbohydrazones

Aleksandra R. Božić [a], Nenad R. Filipović [b], Tatjana Ž. Verbić [c], Miloš K. Milčić [c], Tamara R. Todorović [c], Ilija N. Cvijetić [d], Olivera R. Klisurić [e], Marina M. Radišić [f], Aleksandar D. Marinković [f,*]

[a] *Belgrade Polytechnic, Brankova 17, 11000 Belgrade, Serbia*
[b] *Faculty of Agriculture, University of Belgrade, Nemanjina 6, Belgrade, Serbia*
[c] *Faculty of Chemistry, University of Belgrade, Studentski trg 12-16, 11000 Belgrade, Serbia*
[d] *Innovation Center of the Faculty of Chemistry, University of Belgrade, Studentski Trg 16, 11000 Belgrade, Serbia*
[e] *Department of Physics, Faculty of Sciences, University of Novi Sad, Novi Sad, Serbia*
[f] *Faculty of Technology and Metallurgy, University of Belgrade, Karnegijeva 4, Belgrade, Serbia*

Received 7 May 2017; accepted 22 August 2017
Available online 1 September 2017

KEYWORDS

Solvatochromism;
LSER;
Photoisomerization;
Intramolecular charge transfer;
Quantum chemical calculation

Abstract The substituent and solvent effect on intramolecular charge transfer (ICT) of twelve monocarbohydrazones (mCHs) were studied using experimental and theoretical methodology. The effects of specific and non-specific solvent–solute interactions on the UV–Vis absorption maxima shifts were evaluated using linear free energy relationships (LFERs) principles, *i.e.* using the Kamlet-Taft and Catalán models. Linear free energy relationships in the form of single substituent parameter equation (SSP) was used to analyze substituent effect on UV–Vis, NMR and pK_a change. According to crystallographic data and quantum chemical calculations, the *trans* (*E*) form was found to be more stable. A photochromism of compounds with 2-hydroxyphenyl and 2-pyridylimino groups substituted at imine carbon atom results in *E*/*Z* isomerization due to creation of intermolecular hydrogen bond in *E* and *Z* form, respectively. Multiple stage mass spectrometry (MS-MS^n) analysis was applied to define main fragmentation pathways. Furthermore, the experimental findings were interpreted with the aid of *ab initio* MP2/6–311 G(d,p) and time-dependent density functional (TD-DFT) methods. TD-DFT calculations were performed to quantify the efficiency of intramolecular charge transfer (ICT) with the aid of the charge-transfer distance (D_{CT}) and the amount of transferred charge (Q_{CT}) calculation. It was found that both

* Corresponding author.
E-mail address: marinko@tmf.bg.ac.rs (A.D. Marinković).
Peer review under responsibility of King Saud University.

Production and hosting by Elsevier

http://dx.doi.org/10.1016/j.arabjc.2017.08.010

substituents and solvents influence electron density shift *i.e.* extent of conjugation, and affect ICT character in the course of excitation.

1. Introduction

Hydrazones constitute a privileged class of organic compounds which possess biological properties (Alam et al., 2014) as well as wide range of analytical and industrial applications (Taploo and Dhar, 1982). It is known that their coordination behavior depends on *p*H of the medium, nature of the substituent and position of hydrazone group relative to other nucleus (Swathy et al., 2016). Their ability to bind and stabilize different metal ions in various oxidation states makes them exquisite compounds for the design of coordination systems with biological activity (Patel, 2010), as well as reagents in analytical chemistry (Rosales, 1985). Their biological activity may be due to the ability of the ligands to form stable complexes with the metal ions which the fungus needs for its metabolism (Al-Hazmi and Metwally, 2017).

Carbohydrazide ($H_2NNHCONHNH_2$; dhO) is a analog of semicarbazide ($H_2NCONHNH_2$), and compound which possesses two reactive hydrazine groups capable of condensation with one or two carbonyl compounds to produce mono- and bis-carbohydrazones, respectively (Božić et al., 2016). Synthetic capabilities of dhO offer wide possibilities for tailoring different imino compounds which are progressively recognized not only as chelating agents but also as functional molecules, for example, for selective anion binding (Rubčić et al., 2014).

Monocarbohydrazones (mCHs) derived from carbohydrazide are still poorly investigated. Flexible structure and properties of mCHs was described in the literature (Bacchi et al., 1999; Novak et al., 2012; Okawara et al., 2006; Zelenin et al., 1999), but all these reports lack detailed structural and theoretical study. Only salicylidene carbohydrazide asymmetric hydrazones have been subjected to a detailed structural characterization in solution (Novak et al., 2012). It was shown that these derivatives were capable of ring-chain tautomerism in DMSO-d_6 (Zelenin et al., 1999), while chelating nitrogen-donor ligand methyl 4-pyridyl ketone carbonohydrazone has been used for the synthesis of a luminescent cationic porous framework (Karmakar et al., 2014). Some mono and biscarbohydrazones and their metal complexes possess antimicrobial activity against Gram-positive and Gram-negative bacteria (Bacchi et al., 1999), antifungal activity (Kothari and Sharma, 2010), antioxidant and anticancer activity (Abu El-Reash et al., 2013, 2014; El-Gammal et al., 2012). The most interesting feature of this kind of polydentate ligand system is the coordination versatility, which arises from the tautomeric equilibrium between keto and enol forms. Structural characterization of carbohydrazide derived hydrazones complexes exhibit the common coordination mode of the enol (Bacchi et al., 1996; Lozan et al., 2003) and keto form (Kogan et al., 2005; Sutradhar et al., 2014). Based on the results of the first systematically published investigation of antitumor activity of three quinoline contained mCHs and their corresponding bis-structural counterparts showed better activity than mCHs and induce cell death in the 2D AsPC-1 (pancreatic adenocarcinoma cancer stem cells) (Božić et al., 2016). Also, the screening of antioxidant and antimicrobial of fourteen *mono*- and *bis*-carbohydrazone ligands revealed that phenyl 2-pyridyl ketone carbohydrazone showed good antioxidant activity, and quinoline based mCHs was the best antimicrobial agents with respect to both Gram-positive and Gram-negative bacteria (Božić et al., 2017).

In this work, we report the synthesis of twelve mCHs (**1**–**12**) (Scheme 1), which were characterized using UV–Vis, NMR and MS-MS^n methods. Additionally, pK_a values of synthesized compounds were experimentally determined. The contributions of the solvent–solute interactions on the shifts in UV spectra were investigated by the use of linear solvation energy relationships (LSER) (Rančić et al., 2019). The effects of solvent dipolarity/polarizability and solvent–solute hydrogen bonding interactions were evaluated by means of the LSER principles using Kamlet-Taft model (Kamlet et al., 1981). The effects of solvent dipolarity, polarizability, and solvent–solute hydrogen bonding interactions were evaluated by means of the linear solvation energy relationship (LSER) model of Catalán (Catalán, 2009).

The linear free energy relationship (LFER) principles were applied to get an insight into factors influencing ^{13}C and ^{1}H NMR chemical shifts, ν_{max} and pK_a value. Hammett or single substituent parameter equation (SSP) was used to analyzed the transmission of electronic substituent effects (Hansch et al., 1995).

Experimentally obtained chemical properties of mCHs (Scheme 1) have been compared to results obtained by computational methods. The computational studies include MP2 geometry optimization, time-dependent density functional theory calculations (TD-DFT) of absorption spectra and electronic transitions and evaluation of Intramolecular Charge Transfer (ICT) by calculation of D_{CT} and Q_{CT} values, as well as Atoms in Molecules (AIM) analysis of intramolecular hydrogen bonding in the ground state.

2. Experimental

2.1. Materials

Details on materials used in experimental work are given in Supplementary material.

2.2. Synthesis of monocarbohydrazones

General procedure for the synthesis of monocarbonohydrazones **1**–**12** is shown in Scheme 1. mCHs **1**–**9** were prepared by reactions between dhO (1 mmol) and appropriate aldehydes and ketones (0.5 mmol) in water (10 ml) at room temperature with one drop of hydrochloric acid. Reaction mixture was stirred for 2 h and the resulting precipitate was collected by

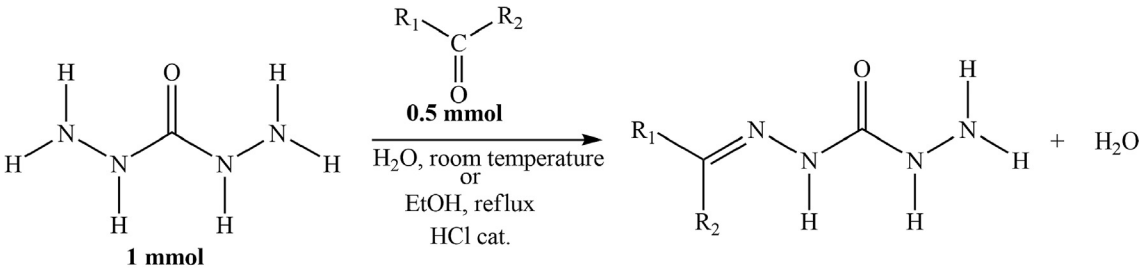

Compound	R_1	R_2	Compound	R_1	R_2
1	Phenyl	H	**7**	2-Pyridyl	Me
2	2-Hydroxyphenyl	H	**8**	3-Pyridyl	Me
3	2-Pyridyl	H	**9**	4-Pyridyl	Me
4	3-Pyridyl	H	**10**	8-Quinolyl	H
5	4-Pyridyl	H	**11**	2-Quinolyl	H
6	Phenyl	Me	**12**	8-Hydroxy-2-Quinolyl	H

Scheme 1 Schematic overview of mCHs syntheses and list of synthesized mCHs.

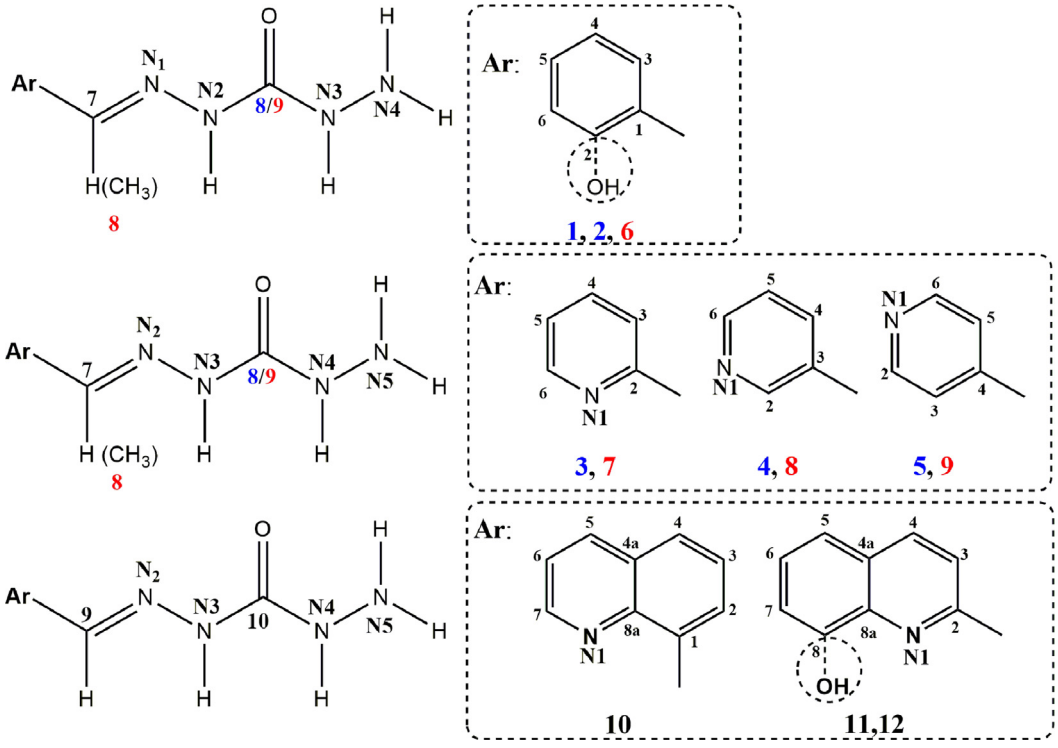

Scheme 2 Numbering of atoms in mCHs used in NMR.

filtration and recrystallized from a suitable solvent. Compounds **10**–**12** were synthesized in analogous manner (molar ratio) applied for syntheses of **1**–**9** using ethanol as solvent (30 mL) under reflux for 3 h. The compounds **1** and **6** (Zelenin et al., 1999), **2** (Novak et al., 2012), **3** and **7** (Božić et al., 2017), **5** (Okawara et al., 2006), **9** (Karmakar et al., 2014), and **10**–**12** (Božić et al., 2016) are known compounds. Purity of synthesized compounds was verified by elemental analysis and NMR spectroscopy (Supplementary material), and obtained results for known substances are in agreement with literature data. List of synthesized compounds with numeration of the atoms of interest is given in Table S1 and Scheme 2.

2.2.1. 3-pyridinecarboxaldehyde carbohydrazone (4)

Yield: 60%. White crystals suitable for single crystal XRD were obtained after recrystallization compound from absolute ethanol. M.p. 166–167 °C. Elemental analysis calcd. for $C_7H_9N_5O$ (Mw = 179.18 g mol^{-1}): C, 46.92; H, 5.06; N,

Table 1 Crystallographic data and refinement parameters for compounds **5** and **9**.

	5	**9**
Chemical formula	$C_7H_9N_5O$	$C_8H_{11}N_5O$
M_r	179.19	193.22
Crystal system, space group	Monoclinic, $P2_1/c$	Monoclinic, $P2_1/c$
a, b, c (Å)	8.5421 (7), 9.7341 (5), 10.4508 (7)	8.3793 (6), 9.9529 (4), 11.1145 (6)
β (°)	97.759 (7)	91.626 (6)
V (Å^3)	861.02 (10)	926.56 (9)
Z	4	4
μ (mm^{-1})	0.10	0.82
Crystal size (mm)	0.49 × 0.40 × 0.19	0.46 × 0.33 × 0.28
Absorption correction	Multi-scan CrysAlis PRO (Oxford Diffraction Ltd., 2009) Empirical absorption correction using spherical harmonics, implemented in SCALE3 ABSPACK scaling algorithm	
T_{min}, T_{max}	0.985, 1.000	0.988, 1.000
No. of measured, independent and observed [$I > 2\sigma(I)$] reflections	3555, 1938, 1312	5963, 1806, 1478
R_{int}	0.020	0.024
θ values (°)	θ_{max} = 29.0, θ_{min} = 2.9	θ_{max} = 72.5, θ_{min} = 5.3
$R[F^2 > 2\sigma(F^2)]$, $wR(F^2)$, S	0.048, 0.109, 1.06	0.042, 0.122, 1.08
No. of parameters	134	144
No. of restraints	0	0
Weighting scheme	$w = 1/[\sigma^2(F_o^2) + (0.0424P)^2 + 0.0087P]$ where $P = (F_o^2 + 2F_c^2)/3$	$w = 1/[\sigma^2(F_o^2) + (0.0569P)^2 + 0.1592P]$ where $P = (F_o^2 + 2F_c^2)/3$
H-atom treatment	H atoms treated by a mixture of independent and constrained refinement	
$\Delta\rho_{max}$, $\Delta\rho_{min}$ (e Å^{-3})	0.11, −0.18	0.14, −0.15

39.09%, Found: C, 46.76; H, 5.11; N, 38.96%. IR (KBr, cm^{-1}): 3308 s (NH_2), 3211 s (NH), 1675 vs (C═O), 1638 m (C═N). ^{1}H NMR (500 MHz, DMSO-d_6, δ (ppm): 4.09 (s, 2H, H-N5); 7.39 (dd, 1H, H–C5, $^3J_{5,4}$ = 7.95 Hz, $^3J_{5,6}$ = 4.75 Hz); 7.87 (s, 1H, H-C7); 8.063–8.319 (br.m.ovlp., 2H, H–C4,H-N4, $^3J_{4,5}$ =7.95 Hz); 8.51 (dd, 1H, H–C6, $^3J_{6,5}$ = 4.75); 8.86 (d, 1H, H–C2); 10.56 (s, 1H, H–N3). ^{13}C NMR (126 MHz, DMSO-d_6, δ (ppm): 123.67 (C5); 130.67 (C3); 133.25 (C4); 137.00 (C7); 148.28 (C2); 149.64 (C6); 156.95 (C8).

2.2.2. Methyl 3-pyridyl ketone carbohydrazone (*8*)

White solid was recrystallized from absolute methanol. Yield: 90.09%. M.p. 190–191 °C. Elemental analysis calcd. for $C_8H_{11}N_5O$ (Mw = 193.21 g mol^{-1}): C, 47.73; H, 5.74; N, 36.25%, Found: C, 47.66; H, 5.82; N, 36.25%. IR (KBr, cm^{-1}) ν_{max}: 3314 m (NH_2), 3264 m (NH), 3032 w (CH_{aryl}), 1672 vs (C═O), 1649 m (C═N). ^{1}H NMR (500 MHz, DMSO-d_6, δ (ppm): 2.20 (s, 3H, H-C8); 4.10 (s, 2H, H–N5); 7.37 (ddd, 1H, H–C5, $^3J_{5,4}$ = 8.1 Hz, $^3J_{5,6}$ = 4.7 Hz); 8.12 (s, 1H, H-N4); 8.27 (d, 1H, H–C4, $^3J_{4,5}$ = 8.1 Hz); 8.51 (dd, 1H, H–C6, $^3J_{6,5}$ = 4.7 Hz); 9.03 (d, 1H, H–C2); 9.62 (s, 1H, H–N3). ^{13}C NMR (126 MHz, DMSO-d_6, δ (ppm): 12.86 (C8); 123.19 (C5); 133.36 (C3); 133.65 (C4); 142.57 (C7); 147.37 (C2); 149.15 (C6); 157.46 (C9).

2.3. Methods

2.3.1. Elemental analysis, FTIR, NMR and UV spectroscopy

Elemental analyses (C, H, N) were performed by the standard micromethods using the ELEMENTAR Vario EL III CHNS/O analyzer. Fourier-transform infrared (FTIR) spectra were obtained using FTIR BOMEM MB 100 in the form of KBr pellets. FTIR spectra were recorded in the transmission mode between 400 and 4000 cm^{-1} with a resolution of 4 cm^{-1}. Abbreviations used for IR spectra: vs very strong; s, strong; m, medium; w, weak. All NMR spectral measurements were performed on a Bruker Avance III 500 spectrometer equipped with a broad-band direct probe. The spectra were recorded at room temperature in DMSO-d_6. Chemical shifts are given on δ scale relative to tetramethylsilane (TMS), as internal standard for ^{1}H and ^{13}C, or relative to urea (77.0 ppm) as the external standard for recording ^{15}N NMR spectra. Coupling constants (J) were expressed in Hz. Abbreviations used for NMR spectra: s, singlet; dd, doublet of doublets; ddd, double double doublet. The UV absorption spectra were measured in a range 200–600 nm by using Shimadzu 1700 UV/Vis spectrophotometer. The UV–Vis spectra were recorded at a concentration of 1×10^{-5} mol L^{-1}. Three measurements were performed and mean value was presented.

2.3.2. X-ray diffraction analysis

The diffraction data for compounds **5** and **9** were collected at room temperature on Rigaku (Oxford Diffraction) Gemini S diffractometer using program package CrysAlis CCD with graphite-monochromated CuKα (λ = 1.54184 Å) for **9** and MoKα (λ = 0.71071 Å) radiation for **5**. The data reduction was performed with program package CrysAlis RED (Oxford Diffraction Ltd., 2009). The space group determinations were based on an analysis of the Laue class and the systematically absent reflections. Collected data were corrected for absorption effects by multi-scan absorption correction using spherical harmonics as implemented in SCALE3 ABSPACK scaling algorithm (SCALE3 ABSPACK).

The structures were solved by direct methods using SHELXT (Sheldrick, 2015) and refined by full-matrix

least-squares procedures on F^2 using SHELXL-2014/6 program (Sheldrick, 2015). For both compounds non-hydrogen atoms were refined anisotropically, the CH hydrogen atoms were included on calculated positions riding on their attached atoms with fixed distances of 0.93 Å (CH) and 0.96 Å (CH_3). At the final stage of the refinement, H atoms attached to N atoms were identified on difference electron density maps and isotropically refined. All calculations were performed using PARST and PLATON (Farrugia, 1997), as implemented in the WINGX (Farrugia, 1999) system of programs. The crystal data and refinement parameters are summarized in Table 1.

Crystallographic data are deposited in the Cambridge Crystallographic Data Centre as supplementary material number CCDC – 1545871 (for **9**) and – 1545872 (for **5**). The CCDC files 1545871–1545872 contain the supplementary crystallographic data. Copies of this information may be obtained free of charge from the Director, CCDC, 12 Union Road, Cambridge, CB21FZ, UK (email: deposit@ccdc.cam.ac.uk or http://www.ccdc.cam.ac.uk).

2.3.3. LSER analysis

The effects of solvent dipolarity/polarizability and solvent–solute hydrogen bonding interactions were evaluated by means of the LSER principles using Kamlet-Taft model given by Eq. (1) (Kamlet et al., 1981):

$$\nu_{max} = \nu_0 + s\pi^* + b\beta + a\alpha \quad (1)$$

where ν_{max} is the absorption frequency maxima, π^* is an index of the solvent dipolarity/polarizability; β is a measure of the solvent hydrogen-bond acceptor (HBA) basicity; α is a measure of the solvent hydrogen-bond donor (HBD) acidity, and ν_0 is the regression value in cyclohexane as reference solvent. The solvent parameters used in Eq. (1) are given in Table S2. The regression coefficients s, b and a in Eq. (1) measure the relative susceptibilities of the absorption frequencies maxima to the solvent effect. The effects of solvent dipolarity, polarizability, and solvent–solute hydrogen bonding interactions were evaluated by means of the linear solvation energy relationship (LSER) model of Catalán (Catalán, 2009), given by Eq. (2):

$$\nu_{max} = \nu_0 + a\mathrm{SA} + b\mathrm{SB} + c\mathrm{SP} + d\mathrm{SdP} \quad (2)$$

where SA, SB, SP and SdP characterize solvent acidity, basicity, polarizability and dipolarity of a solvent, respectively; and a to d are the regression coefficients describing the sensitivity of the absorption maxima to the different types of the solvent–solute interactions. The solvent parameters used in Eq. (2) are given in Table S3.

2.3.4. LFER analysis

The linear free energy relationship (LFER) principles were applied to get an insight into factors influencing ^{13}C and ^{1}H NMR chemical shifts, ν_{max} and pK_a value. Hammett or single substituent parameter equation (SSP) in the form given by Eq. (3) was used to analyzed the transmission of electronic substituent effects:

$$Y = \rho\sigma + h \quad (3)$$

where Y is a substituent–dependent value: ν_{max} or NMR chemical shifts, ρ is the proportionality constant reflecting the sensitivity of the ν_{max} to the substituent effects, σ is the corresponding substituent constant, and h is the intercept (*i.e.* describes the unsubstituted member of the series) (Hansch et al., 1995). The σ values, given in Table S4, correspond to an additive value of the contribution of both polar and π-delocalization effects.

2.3.5. Determination of the pK_a values

Potentiometric titrations, performed by using CRISON pH-Buret 24 2S equipped with CRISON 50 29 microcombined pH electrode (Crison Instruments, SA, Spain), was applied to determine acidity constants, *i.e.* pK_a value, of studied mCHs. The electrode was calibrated by means of a strong acid–strong base titration in 0.1 M NaCl in MeOH: H_2O (1: 1, *v*/*v*), using GLEE, GLass Electrode Evaluation software; (Gans and O'Sullivan, 2000) standard potential E^0 = 397.9 ± 0.2 mV, slope 59.2 ± 0.1 mV, and pK_W 13.84 ± 0.01 were obtained as mean values of four titrations. All compounds were of >95% purity.

2.3.6. MS/MS^n study

The mass spectrometer used was the LTQ XL linear ion trap (Thermo Fisher Scientific, Waltham, MA, USA) with electrospray ionization (ESI). The results were processed using the Xcalibur® version 2.3 (Thermo Fisher) software package. Tuning of the mass spectrometer was performed automatically. MS and MS^n experiments were performed using standards in methanol at a concentration of 10 µg mL^{-1}. Standards were delivered by a syringe pump at a flow rate of 10 µL min^{-1}, and mixed through a T-piece with the LC effluent that contained 99% of methanol and 1% of 10% acidic acid. The mobile-phase flow rate was 0.3 mL min^{-1}. Mass spectra for all the compounds were obtained in positive and negative ESI mode. For all experiments in the positive ESI mode, the source voltage was set at 5 kV. Nitrogen was used as a sheath and auxiliary gas, and values (a scale of arbitrary units in the 0–100 range defined by the LTQ XL system) of their flow rate were 32 and 8 respectively. The capillary temperature was maintained at 350 °C. Capillary voltage and tube lens voltage were set at 6 and 75 V, respectively. In negative ESI mode parameters were set as: source voltage was 4 kV, sheath gas flow rate was 32, auxiliary gas flow rate was 8, capillary voltage was −19 V and tube lens voltage was −142 V. Helium was used as the collision gas in the ion trap. The collision energy values were manually optimized for each compound. The maximum inject time for MS experiments was 50 ms and the number of microscans per scan was 2, while for MS^n experiments, maximum inject time was 100 ms and number of microscans was 3. Full scan mode was used to acquire mass spectra and to select the precursor ions for product ion spectra.

2.3.7. Theoretical calculations

Geometries of all molecular species were optimized in gas phase by the MP2 method using 6-311G(d,p) basis set. In order to find the global minimum on the potential energy surface, multiple geometry optimizations were performed for every compound, with varying rotational torsion angle for increment of 15° and minimizing the energy with respect to all geometrical parameters. The nature of the lowest energy minimum was further confirmed with frequency calculations; no negative frequencies were found. Theoretical absorption spectra are calculated on MP2/6-311G(d,p) optimized geometries using time-dependant (TD) density functional theory

(DFT) method. The TD-DFT calculations were done in solvent DMSO with CAM-B3LYP long range corrected functional (Yanai et al., 2004) and 6-311G(d,p) basis set.

Solvent effect have been simulated with standard static isodensity surface polarized continuum model (IPCM) (Wiggins et al., 2009). The same functional and basis set (CAM-B3LYP/6-311G(d,p)) were used for calculating other ground state properties (HOMO-LUMO gap and orbital densities) in DMSO solution. Qualitative charge transfer indices: the charge-transfer distance (D_{CT}), amount of transferred charge (Q_{CT}), and the value of variation of dipole moment between the ground and excited states (μ_{CT}) were evaluated according to method proposed by Le Bahers et al. (2011).

Atoms In Molecules (AIM) analysis was conducted on compounds 2, 3 and 7. Geometries of both isomers of these compounds were reoptimized in DCM and MeOH (IPCM method) with ωB97X-D functional and 6-311G(d,p) basis set. AIM analysis of ground state wavefunction was performed with Multifwfn program (Lu and Chen, 2012). All quantum chemical calculations were carried out using the Gaussian09 program (Frisch et al., 2009).

3. Results and discussion

3.1. Synthesis and compound characterization

Signals observed in ^{1}H and ^{13}C NMR spectra of all synthesized compounds (Scheme 1) match the number of expected signals of hydrogen and carbon atoms, and showed exceptionally good superposition with given literature data. ^{1}D (^{1}H and ^{13}C) and ^{2}D (COSY, NOESY, ^{1}H–^{13}C HSQC and ^{1}H–^{13}C HMBC) spectra of all new compounds and ^{1}D (^{1}H and ^{13}C) spectra of known compounds are shown in Figs. S1–S26 together with the atom numbering scheme (Table S1 and Scheme 2). The spectra of substances that were published in our previous papers (Božić et al. 2016; Božić et al. 2017) are not shown. Elemental analysis results were within ±0.4% of the theoretical values. In the IR spectra of the monocarbohydrazones the absorptions between 1679–1696 cm^{-1} were assigned to the ν(C═O) stretching, δ(N─H) and ν(C─N) vibrations due to contributions of both amide(I) and amide(II) modes, while the absorption between 1604–1640 cm^{-1} is assigned to the ν(C═N) vibration. Absorptions between 3198–3316 cm^{-1} were attributed to the $\nu(NH_2)$ vibration in the spectrum of the mCHs (Božić et al., 2016).

It is known that hydrazones can adopt *E* or *Z* configuration around C═N double bond (Lin et al., 2012). Analysis of NMR chemical shifts was performed in order to get deeper insight into conformational arrangement of molecules and effect of intramolecular hydrogen bonds (example given for comps. **2** and **3** on Figs. S27 and S28, respectively) to solvatochromism and photochromism of mCHs. The chemical environment of the **N3-H (N2-H** for **1**, **2** and **6)** (Table S1 and Scheme 2) atom is different in the *E* isomer from that for the *Z*. mCHs show a peak in the range 10.64–10.76 for compounds **3**–**5** and **10**, 9.62–9.76 for compounds **7**–**9**, 10.84–10.88 for compounds **11** and **12** assigned to chemical shift of **N3-H** atom. Also, chemical shift of **N2-H** atom was found to be in the range 10.30–10.40 for compounds **1** and **2** and 9.50 for compound **6**. It was previously described that the downfield shift of **N3-H** atoms, found at 13.20 ppm, for the *Z* isomer of 2-benzoylpyridine carbohydrazone is consistent with deshielding effect due to hydrogen bonding between the **N3-H** atom and the aromatic nitrogen in 2-pyridyl group (Božić et al., 2017).

As an example, chemical shifts of new compounds **4** and **8** were assigned by combined use of 1-D (^{1}H and ^{13}C, Figs. S7, S8, S19 and S20), and 2-D NMR spectroscopy (COSY, NOESY, ^{1}H-^{13}C HSQC, ^{1}H-^{13}C HMBC given in Figs. S9–12 and S21–24, respectively). In order to assess conformation of studied compounds in solution, 2-D NOESY sequence was applied, and results confirmed that compound **3**, **4** and **8** exists in *E* form in DMSO solution. The *E* configuration of the hydrazone moiety in the **3**, **4** and **8** can be evidenced from 2D NOESY spectra (Figs. S5, S10 and S22) by cross-correlation of H-atoms at **C7** and **N3** for comp. **3** and **4**, and **C8** and **N3** for comp. **8**. Also, additional evidence was obtained from 2D ^{15}N-HMBC spectrum of **3** (Fig. S6) (Božić et al., 2017), where no observable connectivity between H-atom at **N3** and **N1** nitrogen indicate *E* conformation. Otherwise, appropriate correlation of **N3-H** and **N1** in *Z* conformation would be expected due to formation of intramolecular hydrogen bonding in pseudo six-membered ring (Fig. S28) (Jansma et al., 2007).

It was also shown that creation of three-centered hydrogen bonds in DMSO/compound **2** system contribute to the higher stability of obtained complex by 11.21 kJ mol^{-1} (Novak et al., 2012). Therefore, NMR results proved that studied mCHs occupy more stable *E* conformation in DMSO.

3.1.1. Crystal structures of compounds 5 and 9

An ORTEP (Farrugia, 1997) drawings of the molecular structures of **5** and **9** are depicted in Fig. S29, while selected bond distances, bond angles and torsion angles within these compounds are given in Table S5. Compounds **5** and **9** crystallize in the monoclinic centrosymetric $P2_1/c$ space group (Table 1) and have very similar structures in the solid state (Fig. 1, Table S5). The molecules of both compounds are slightly distorted, the maximum displacement from planarity in value of the dihedral angle N5—N4—C7—N3 is not greater than 8.53 (17)°. As illustration the maximum difference can be noticed in comparison of C3—C6 bond length (1.483(2) Å in

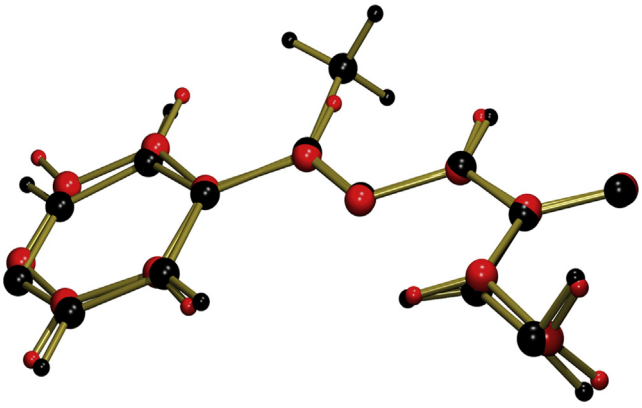

Fig. 1 Structural superposition of **5** (red atoms) with **9** (black atoms).

Table 2 Ground state energies of optimized structures of compounds **1**–**12**.

Compound/isomer	Energy (Hartree)	ΔE (kcal)
1/*E*	−603.2831718	−2.31
1/*Z*	−603.279484	0.00
2/*E*	−680.2559807	−9.69
2/*Z*	−680.2405457	0.00
3/*E*	−621.0584152	0.00
3/*Z*	−621.0618412	−2.15
4/*E*	−621.0562028	
5/*E*	−621.0563581	
6/*E*	−642.4700374	0.00
6/*Z*	−642.4706955	−0.41
7/*E*	−660.3772243	0.00
7/*Z*	−660.3780726	−0.53
8/*E*	−660.3725635	−1.82
8/*Z*	−660.3696592	0.00
9/*E*	−660.3731491	−2.17
9/*Z*	−660.3696854	0.00
10/*E*	−774.6807102	
11/*E*	−774.6834456	
12/*E*	−849.9142461	

9 and 1.458(2)Å in **5**) and N2—C3—C6 bond angle (115.42(14)° in **9** and 120.41(14)° in **5**).

3.1.2. Geometry optimization of mCHs

Carbohydrazones might exist in keto/enol tautomeric forms, and also they could adopt *E* or *Z* configuration around the C=N bond (Zelenin et al., 1999). The state of equilibria depends on energy of appropriate form, solvent/solute interactions and intra/intermolecular hydrogen bonding. In accordance to the study on *E*/*Z* isomerization and keto-enol tautomerization of some mCHs in a mixed DMSO/water mixtures (Božić et al., 2017), theoretical and experimental study of mCHs showed significantly higher stability of keto form.

Results of theoretical calculations at MP2/6-311G(d,p) level are shown in Table 2, S6 an S7. Energies of optimized structures in DMSO are given in Table 2 and selected geometrical parameters, including bond distances, bond angles and dihedral angles are shown in Tables S6 and S7. Similar results were obtained for gas phase calculation.

According to the results from Table 3, it is indicative that *E* isomer is more stable for compounds **1**, **2**, **4, 5**, **8**–**12**, while three mCHs, *i.e.* **3**, **6** and **7**, could favourably occupy *Z* configuration. The compounds **3** and **7** with 2-pyridyl ring present in imine part of molecule showed somewhat higher stability in *Z* form (Fig. S28). These results indicate that two effects: intramolecular hydrogen bonding (major effect) and steric influences of methyl group (to a lower extent), in compounds **6** and **7**, contribute to the higher stability of *Z* form.

Structural variation, *i.e.* geometrical isomerization and change in torsional angles (Scheme 3), defined by out-of-plane rotation of substituent with respect to imino bond and rotation around single bonds, were also analyzed in order to complete the whole picture on geometrical arrangement of mCHs. The measured dihedral/torsional angles of interest for analysis of geometrical feature of investigated compounds are given in Scheme 3.

Elements of the optimized geometries of investigated compounds, obtained by the use of MP2/6-311G(d,p) method for *E* and *Z* isomer are given in Tables S6 and S7. It can be seen that geometric features of the studied *E*/*Z* isomers follow the appropriate trend of geometry parameter change *versus* electronic effect of the groups present at imino part of the molecule. Consideration of the torsional angles α, β, χ and δ (Tables S6 and S7) and their changes indicates that introduction of substituent induces small changes of the analyzed values.

Table 3 Absorption frequencies of the *E* isomer of mCHs.

Solvent/compound	$\nu_{max} \times 10^{-3}$ (cm^{-1})											
	1	2	3	4	5	6	7	8	9	10	11	12
EtOH	34.36	31.25	33.87	33.57	33.78	36.49	34.32	35.29	34.60	30.43	32.56	30.57
MeOH	34.60	31.49	34.05	33.66	33.95	36.49	34.52	35.41	34.73	30.81	32.88	30.85
1-PrOH	34.34	31.34	33.93	33.69	33.75	36.48	34.34	35.03	34.54	30.57	32.56	30.60
1-BuOH	34.35	31.34	34.05	33.67	33.83	36.46	34.35	35.22	34.52	30.56	32.67	30.58
i-BuOH	34.55	31.30	34.01	33.71	33.74	36.46	34.45	35.02	34.56	30.45	32.75	30.57
1-PeOH	34.22	31.28	33.87	33.62	33.65	36.50	34.20	34.97	34.66	30.58	32.65	30.58
i-PeOH	34.28	31.29	34.04	33.74	33.81	36.47	34.28	35.20	34.43	30.55	32.52	30.57
2ME	33.65	31.44	34.06	33.63	33.68	36.25	33.71	35.08	34.64	30.35	32.44	30.23
2CE	34.21	31.59	34.08	33.97	34.12	36.55	34.01	35.18	34.69	30.54	32.55	30.44
Water	35.59	32.04	34.39	33.59	34.30	36.90	35.98	35.86	35.84	31.47	32.57	31.41
AcN	34.96	31.74	33.95	33.98	34.41	36.49	34.23	35.58	34.95	30.61	33.30	30.82
Chl	34.72	31.20	33.97	33.96	34.69	36.49	34.39	35.6	34.36	31.03	32.71	30.95
Et_2O	34.35	31.48	33.82	33.51	34.02	36.44	34.39	35.60	35.70	30.18	33.10	30.22
THF	34.01	30.99	33.66	33.47	33.80	35.84	34.69	35.44	34.82	29.96	32.79	30.47
Dioxane	34.62	31.27	33.73	33.59	34.25	34.52	34.61	35.31	34.50	30.16	32.85	30.09
2-Py	33.92	31.41	33.59	33.02	33.35	35.85	33.89	34.57	34.75	29.82	32.48	29.84
EtAc	34.22	31.68	33.69	33.85	33.64	36.29	34.12	35.28	34.53	30.34	32.82	30.41
DCM	35.09	31.29	34.13	33.94	35.52	36.49	34.24	35.33	35.29	30.51	32.67	30.64
NMP	33.79	31.00	33.54	32.68	33.43	35.80	33.77	34.73	34.38	29.52	32.47	30.30
DMF	33.82	31.15	33.59	33.26	33.55	35.35	33.73	34.75	34.34	29.91	32.44	30.30
DMSO	33.78	31.05	33.51	33.05	33.53	35.33	33.67	34.77	33.90	29.93	32.37	29.84
DMA	33.68	31.25	33.31	33.57	33.78	35.38	33.47	34.62	34.17	29.97	32.62	30.21

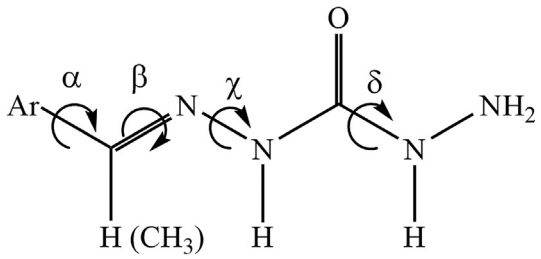

Scheme 3 Defined dihedral angles used in conformational analysis.

An appropriate change of the aryl-imine bond length C2–C7 (or C3-C7; C4-C7; C7-C9 or C2-C9) (for numbering scheme see Table S1 and Scheme 2) indicates that two opposite electron accepting effects operate in both arylidene (benzylidene) part and carbonyl groups in carbohydrazide part of molecule. These effects cause appropriate geometry adjustment as a response to electronic demand of the electron deficient environment. Due to this, the normal carbonyl groups polarization is suppressed and causes a slight bond length decrease. Greater extent of the π,π-delocalization causes decrease in the C2—C7 bond length, which is a part of the arylidene imino conjugated system. The introduction of electron-donor substituent, considering compounds **2** and **12** with respect to **1** and **11**, respectively, causes small decrease of both C2—C7 and carbonyl group bond length. Electro-donating hydroxy group compensate strong electron-accepting effect of "aza" group and low effect of imino nitrogen in that way an increase of π-resonance interaction is a consequence. The opposite trend is exhibited when electron-acceptor is present, considering series **3**–**5** and **7**–**9** with respect to **1** and **6**, respectively. The results indicated on distance dependent inductive effect of "aza" group on bond length change: larger effect/longer bond of 2-pyridyl group (comps. **3** and **7**) was observed with respect to 3- and 4-pyridyl susbstituted compounds. Exception was noticed for compound **5**, small increase of this bond with respect to **4** was noticed, as a result of strong directional electron-withdrawing effect of "aza" group and methyl group at imine carbon. Steric effect of methyl group cause appropriate disturbance of π-electron delocalization caused by substituent.

The results are different for the *Z* form of compounds **7**–**9** with only moderate differences in the length of rotational bonds and small deviation from planarity. The deviation from the planarity decrease with increasing electron-acceptor ability of the benzylidene substituent. Comparison between the theoretically predicted geometries and the experimental ones, obtained from crystallographic study for compounds **5** and **9**, indicate good accordance of obtained results confirming validity of the applied methodology.

3.1.3. MS/MS^n analysis

In the MS spectra in positive and negative mode some protonation/deprotonation processes should indicate prevailing basic/acidic sites in the structure of investigated mCHs. Based on the pK_a value prediction (ADMET Predictor, 2015) (Fig. S30) studied mCHs contain Lewis acidic and basic sites which could show structure dependent fragmentation paths in in positive and negative electrospray ionization mode. Positive ions observed in MS spectra (Figs. S31–S36) are generated mainly by bonding of the H^+ ion to the terminal amine site, as the most basic one. Most of the investigated molecules display similar fragmentation paths but intensities of the protonated molecular ions and thus their fragments are different.

For all studied compounds common fragmentation behavior was the loss of the H_2NNH_2 group. Main fragmentation path of the compounds **3**–**5**, **7**–**9**, **11** and **12** was similar, loss of the H_2NNH_2 group in the first fragmentation step, loss of –CO in the second fragmentation step and in the third the loss of N_2. Compounds **2**–**4** and **7**–**9** beside the loss of the H_2NNH_2 group in the first fragmentation step also generated a fragment obtained by the loss of H_2NNCO group.

For the compounds **6**–**9**, which have common fragmentation scheme, when regarding the intensities of the observed fragments compound **7** differs. For this compound intensity of the molecular ion is weakest in comparison to the compounds **6**, **8** and **9** and its fragmentation occurs already in the ionization source. Also, for the compound **2** first fragmentation step was found to be very similar to the fragmentations observed for compounds **6**–**9** but intensities of the observed fragments were different. For example, fragment obtained in the first fragmentation step of the compound **2** obtained by the loss of 58 (Fig. 2), and was much more abundant in comparison to the same fragment observed for the compounds **6**–**9** (Figs. S31 and S33). Because this fragment was more stable its further fragmentations were possible. Reason for different intensities of molecular ions and subsequent fragments lies in the influence of electronic effect of arylidene part of the fragments subjected to further fragmentation.

Mass fragmentation of deprotonated molecular ion was quite simple and reflect the most acidic hydrogen removal. Negative MS mode reflects ability of Lewis acidic sites of the mCHs-H molecules to deprotonation processes, and their influence on fragmentation paths. $[mCHs\text{-}H]^-$ ions are generated by dehydrogenation of acidic OH group (**2** and **12**) or amide proton in the other compounds. The lowest intensity of the deprotonated molecular ions was found for **1**, **7** and **10**. For most of the compounds fragmentation occurred already in ionization source. For the compounds **2** and **12** intensities of fragments obtained in the ionization source were even more abundant then the deprotanated molecular ion. Common fragmentation scheme for all the compounds is presented at the Fig. S36. All the compounds in the first fragmentation step loos -NHNHCO group and in the second fragmentation step nitrogen expulsion occured.

In general, fragmentation of studied compound is sensitive to the appropriate proton-donating/proton-accepting capabilities of the particular sites which proved that local electronic density distribution is an important factor determining fragmentation mode of studied compounds.

3.2. Spectral properties of mCHs

The aim of this part of study was devoted to analysis of photophysical properties of mCHs based on results of LSER and LFER multiparameter treatment of UV–Vis and NMR data. Usefulness of the UV–Vis spectroscopy is given in Supplementary material.

It was described that absorbance bands at 235–280 nm of *E* isomer was assigned to π-π^* and n-π^* (Beraldo et al., 2001)

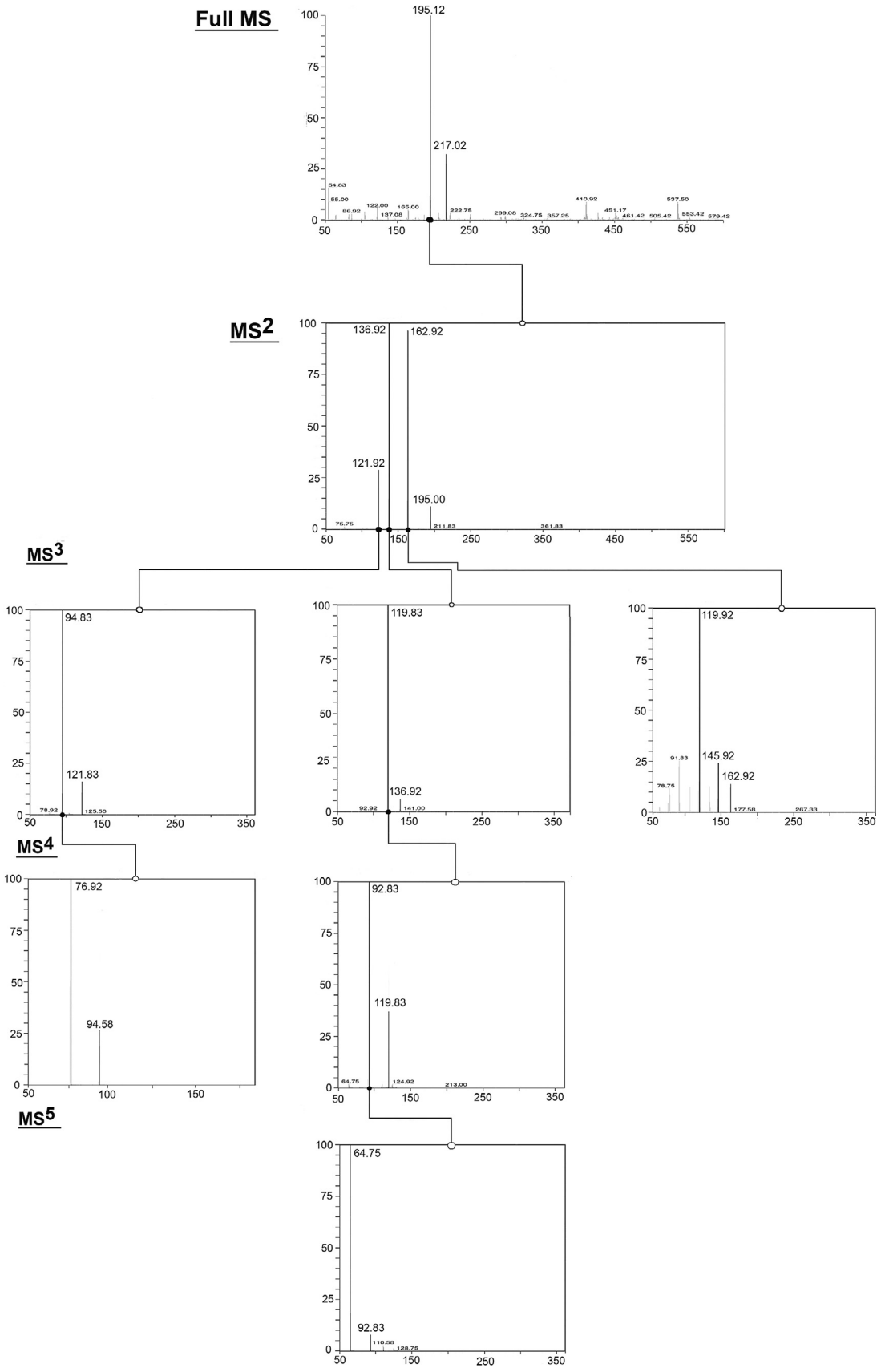

Fig. 2 Multiple stage fragmentation spectra (MS-MS^5) obtained for the compound **2**.

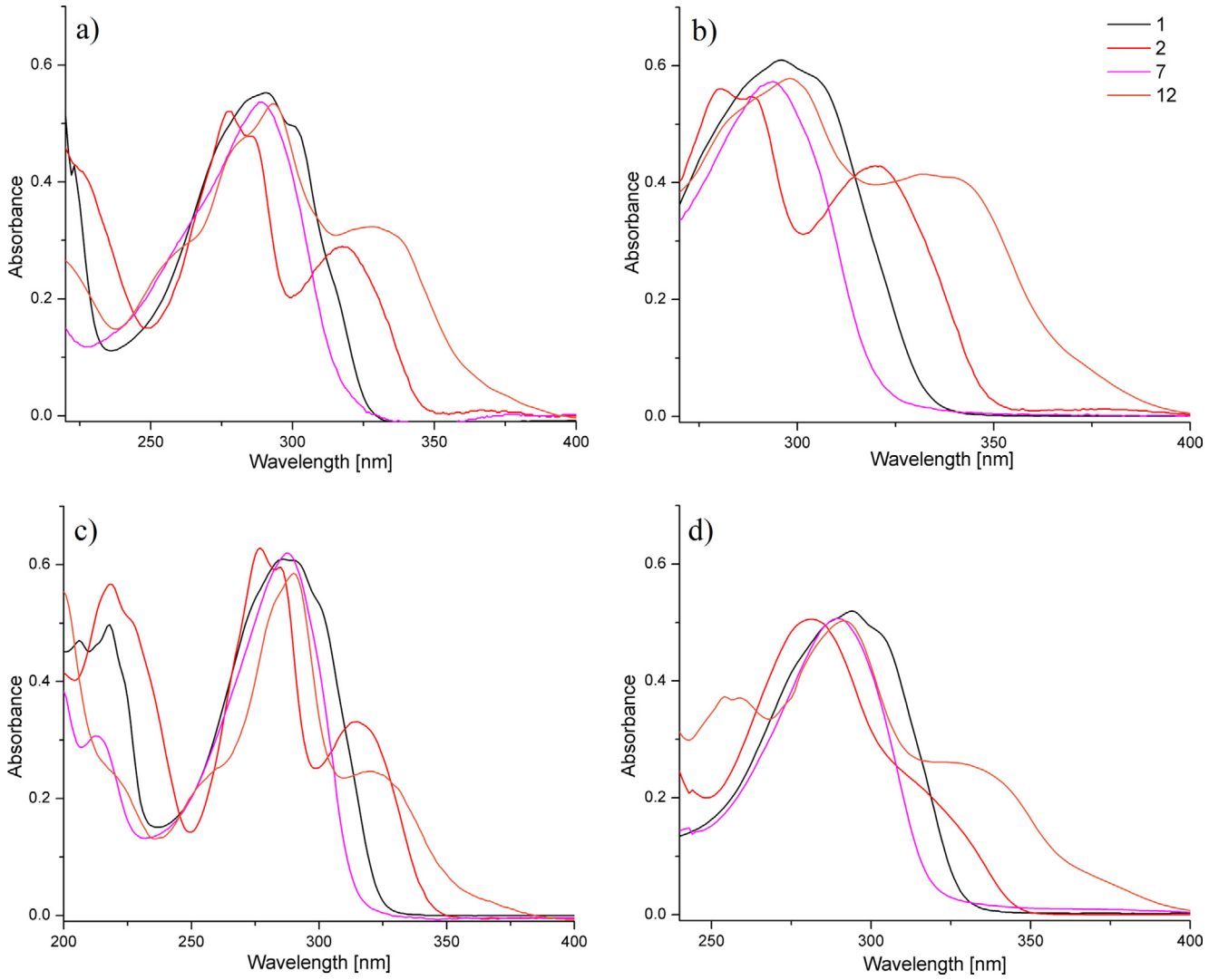

Fig. 3 Absorption spectra of compounds **1**, **2**, **7** and **12** in (a) EtOH, (b) DMSO, (c) AcN and d) THF.

transitions for pyridine derivates of semicarbazones as an analogs of mCHs, and 224–348 nm for quinoline derivates of biscarbohydrazones (Manoj et al., 2008). In the pyridine containing derivatives the π-π^* transitions appeared at lower wavelength (Beraldo et al., 2001). Also, it was shown that the acetylpyridine carbohydrazone exhibit transitions at higher energy than the formylpyridine analogs (Beraldo et al., 2001). According to the literature data with the aid of theoretical calculation it was selected the most significant π-π^* transition from UV–Vis spectra and results are given in Table 3. The absorption spectra of the investigated compounds were recorded in twenty-one solvents of different properties, and the characteristic spectra are shown in Figs. 3 and S37. From the presented UV–Vis spectra in Figs. 3 and S37 simple spectra in the region 250–350 nm were observed, except ones recorded fo comps. **2** and **10**–**12**. The UV–Vis spectra of compounds **4** and **10** in all solvents used are given on Fig. S38.

The data from Table 3 indicate that absorption frequencies depend on both substituent and solvent effect, though the ν_{max} of either electron-donor and electron-acceptor substituted mCHs showed small differences (less than 50 nm), except compounds **10**–**12**. It is expected that introduction of substituent with pronounced electronic effects produces larger variation of ν_{max}, and more pronounced ICT. Accordingly, batochromic (red) shift of the absorption maxima of compounds **1**–**5** and **10**–**12** was observed. Oppositely, hypsochromic shifts of the UV maxima of the mCHs with methyl substituent at imine carbon, *i.e.* compounds **6**–**9**, indicate significance of both electron-accepting capability of benzylidene substituent and steric interference of methyl group. Presence of methyl group cause appropriate conformational adaption which could forces the molecule to slightly deviate from planarity, and thus prevent the higher extent of orbitals stabilization in the course of electronic transition.

3.3. Dependence of compound solvatochromism on its structure

The effect of various types of solvent–solute interactions on the absorption maxima shifts was also interpreted by means of Kamlet-Taft and Catalán LSER models. The correlation analysis was carried out using Microsoft Excel software at confidence level of 95%. The goodness of fit is discussed using the

correlation coefficient (R), the standard error of the estimate (sd), and Fisher's significance test (F). The regression values ν_0, s, a, and b (Kamlet-Taft), and c, d, a, and b (Catalán) fit, at the 95% confidence level, are presented in Tables S8 and 4, respectively.

The negative sign of coefficients s and b, obtained by using Kamlet-Taft concept, for all mCHs indicates batochromic shift of ν_{max} with increasing solvent dipolarity/polarizability and hydrogen-bond accepting capability (Table S8). Opposite and lower magnitude of HBD solvent effect was found, except the negative sign of coefficient a found for compounds **9** and **11**. Detail explanation of the LSER results obtained according to Kamlet-Taft equation was given in Supplementary material.

Separation of non-specific solvent effects, term π^* in Eq. (1), into two terms: dipolarity and polarizability, SP and SdP in Eq. (2), performed according to Catalán equation, are given in Table 4. Results of the quantitative separation of the non-specific solvent effect, defined by coefficients c and d, contribute to advantageous analysis of the solvatochromism of studied compounds.

Correlation results in Table 4 indicate complex influences of both solvent and substituent effects on absorption maxima change reflected in large variation of the contribution of non-specific and specific solvents effects to UV–Vis spectral shifts. The results obtained by the use of Catalán equation provide better understanding of attractive/repulsive solvent/solute interactions and enables an estimation of their appropriate contribution to ν_{max} shift in UV–Vis spectra. Negative values of the coefficients c, d and b, except coefficient d for compound **11**, indicate higher contribution of the dipolarity/polarizability and solvent basicity to the stabilization of the excited state (Papadopoulos et al., 2006). Considering LSER results for compounds **1**, **2** and **6** two trems, dipolarity and HBD solvent effect, dominate for **1** and **6**, while polarizability term, which prevail for **2**, indicate significance of intramolecularly hydrogen bonded pseudo-aromatic structure to larger π-electron mobilty (Fig. S27).

The correlation results from Table 4 imply that the solvent polarizability is the principal factor influencing the shift of ν_{max}, except compounds **1**, **6**, **9** and **10**, while solvent dipolarity is mostly pronounced for compound **6** (somewhat lower values were found for **9** and **10**). Similar trend of the change of correlation coefficients c and d, except for compounds **7–9** regarding coefficient d, was observed in highest values of coefficient s found for 3-pyridyl substituted compounds. These results indicated that higher directional substituent effect of "aza" gorup in 2- and 4-position could compensate solvent effect to some extent. Highest value of coefficient b were found for compounds **5** and **9**, while moderate to low contribution were observed for other mCHs. The change of coefficient b indicate on significance of both position dependent electron-accepting effect of "aza" substituent and structural arrangement, i.e. steric effect of methyl group, which influences proton-donating ability of approrpiate sites at studied mCHs which are susceptible to HBA solvent effect.

Table 4 Results of the correlation analysis of mCHs obtained by using Catalán Eq. (2).

Comp.	h	c	d	b	a	R[a]	Sd[b]	F[c]	Solvent excluded from correlation[d]
1	35.73 ± 0.73	−0.69 ± 1.05	−1.03 ± 0.31	−0.74 ± 0.22	+1.12 ± 0.15	0.93	0.19	21.29	*2ME*, *DCM*, *AcN*,
2	32.29 ± 0.41	−1.19 ± 0.59	−0.07 ± 0.15	−0.33 ± 0.11	+0.52 ± 0.13	0.94	0.09	22.29	*AcN*, *EtAc*, *EtOH*, *THF*
3	34.68 ± 0.30	−1.17 ± 0.47	−0.07 ± 0.14	−0.19 ± 0.13	+0.59 ± 0.10	0.94	0.10	19.00	*MeOH*, *DCM*, *Chl*, *DMA*, *2ME*, *iPeOH*, *iBuOH*
4	36.92 ± 0.40	−3.14 ± 0.53	−0.72 ± 0.19	−0.84 ± 0.13	+0.15 ± 0.18	0.97	0.09	23.95	*H_2O*, *Et_2O*, *2CE*, *DMA*, *Dioxan*, *THF*, *MeOH*, *EtOH*, *NMP*
5	36.87 ± 0.53	−2.33 ± 0.69	−0.62 ± 0.18	−1.28 ± 0.14	−0.34 ± 0.16	0.94	0.13	23.15	*DCM*, *EtAc*, *Et_2O*, *2CE*, *THF*
6	37.57 ± 0.80	−0.33 ± 1.25	−1.83 ± 0.39	−0.13 ± 0.48	+1.37 ± 0.48	0.94	0.18	22.79	*Dioxan*, *2CE*, *AcN*, *DCM*
7	36.90 ± 0.40	−2.49 ± 0.52	−0.99 ± 0.14	−0.40 ± 0.11	+0.28 ± 0.16	0.95	0.10	25.60	*H_2O*, *EtAc*, *THF*, *NMP*, *2ME*, *Et_2O*
8	37.87 ± 0.37	−2.54 ± 0.53	−0.52 ± 0.17	−0.98 ± 0.14	+0.19 ± 0.17	0.94	0.12	24.63	*H_2O*, *1-BuOH*, *iPeOH*, *THF*, *2ME*
9	38.12 ± 0.35	−1.58 ± 0.55	−1.70 ± 0.21	−1.61 ± 0.14	−0.02 ± 0.15	0.97	0.10	54.05	*H_2O*, *Chl*, *EtAc*, *Dioxan*
10	32.06 ± 0.87	−0.27 ± 1.25	−1.59 ± 0.39	−0.76 ± 0.23	+1.15 ± 0.29	0.95	0.18	23.07	*AcN*, *DCM*, *Dioxan*, *2CE*, *Et_2O*, *THF*
11	35.54 ± 0.28	−3.55 ± 0.34	+0.08 ± 0.12	−0.43 ± 0.08	−0.59 ± 0.09	0.95	0.08	27.49	*EtOH*, *EtAc*, *DMF*, *iPeOH*
12	31.78 ± 0.46	−1.20 ± 0.63	−0.20 ± 0.24	−0.56 ± 0.13	+0.59 ± 0.14	0.95	0.11	22.46	*MeCl*, *2CE*, *Et_2O*, *DMSO*, *Dioxan*, *2ME*

[a] Correlation coefficient.
[b] Standard deviation.
[c] Fisher test of significance.
[d] Abbreviation for the solvents are given in Table S2.

Effect of solvent acidity, assigned with *a* term, is of lower significance and showed complex behavior, with the highest value found for compounds **1**, **6** and **10**. Positive values of the coefficient *a*, except compounds **9** and **11**, indicate moderate to low contribution of the solvent acidity to the stabilization of the ground state. Change of the values of coefficient *a* reflects that electron-accepting substituent at azomethine carbon cuse decrease of Lewis basicities of proton-accepting sites at mCHs.

In general, electronic structure of studied mCHs did not belong to typical donor–acceptor (D-A) system which are not able, in conjuction with appropriate structural variation of studied mCHs, to substantially facilitate ICT process. Presented results showed that even some D-A pair was introduced solvatochromic properties were modified in a limited extent.

3.4. LFER analysis of UV–Vis and NMR data

In an attempt to analyze substituent effects on ICT of the investigated mCHs, the LFER principles were applied to the UV–Vis spectral data using Hammett Eq. (3). The correlation results are given in Table 5 and Fig. S39 for *E* isomer.

Generally, the correlation results showed similar susceptibility of the ν_{max} shifts to the electronic substituent effects, and the highest influence was found in water and EtOH. The higher sensitivity of ν_{max} to hydrogen-bonding ability of protic solvent is the factor which contributes to better stabilization of the ground state of studied compounds. Highly dipolar aprotic solvents contribute to somewhat lower sensitivities of ν_{max} to solvent effects. Aprotic solvents mostly behave as proton acceptor and poor anion solvators, and it participate in an effective stabilization of dispersible positive local/overall charges present at investigated molecule. Lower contribution of substituent effects in solvent with higher relative permittivity can be explained by the fact that highly dipolar surrounding medium suppresses electron density shift inducing lower susceptibility of absorption maxima shift to substituent effects. Presented results showed that transmission of substituent electronic effects through π-resonance units takes place by balanced contribution of two modes: through localized π-electronic unit and overall conjugated system of studied mCHs (Rančić et al., 2019).

Furthermore, an LFER analysis has been performed to get a better insight into the influence of the structural and substituent effects on ^{13}C and ^{1}H NMR chemical shifts. LFER principles were applied in the analysis of the substituent effect, defined by σ substituent constant, on the NMR of the carbon and hydrogen atoms of interest. The best correlation results obtained for carbons and hydrogen's nuclei of mCHs and selected literature NMR data for compounds **l1-l3** (Table S4) are presented in Table 6 and Fig. S40.

The general conclusion derived from the ^{1}H and ^{13}C NMR chemical shifts is that all substituents in imino part of molecules influence chemical shifts of the carbon atoms of interest *via* electronic effects. The observed ρ values for these carbons indicate different susceptibilities of the NMR chemical shifts to substituent effects. It is apparent that chemical shifts of C═N and hydrogen atoms showed normal substituent, while reverse substituent effect was observed at C═O carbon. The negative sign of reaction constant, ρ, for C═O atom means reverse behavior, *i.e.* the value of NMR shift decreases although the electron-withdrawing ability of the substituents increases, measured by σ_p. The reverse substituent effect operative at C═O can be attributed to localized π-polarization, which predominates over the extended π-polarization. The π-polarization concept was introduced by Reynolds (Craik and Brownlee, 1983; Reynolds et al., 1983) to explain substituent field effect operative in the side chain of *para*– and *meta*–substituted benzenes (for detail explanation see Supplementary material).

The electron-accepting carbonyl group tends to decrease electron density at the imine group, which result in resonance interaction with para-electron–donating substituents. Electron-donors cause perturbation of electron density at arylidene part which, therefore, acts as π-donor causing increase electron density shift to carbohydrazide moiety. Oppositely, electron-accepting properteis of substituents caused balanced and opposite effect to electronic demand of the rest of molecule. Thus, the transmission of the resonance effect through the extended π-conjugated system in an electron-acceptor substituted mCHs support electron density shift to imine group, and net result is reflected in increased electron density at the C═O carbon.

Additionally, results from inter-correlation of ν_{max} and appropriate NMR data indicates that electron density in both ground and transition states and NMR chemical shifts change under the influence of solvent polarity. In that sense DMSO, AcN and EtOH solvents are considered. Negative slope of linear correlations for ν_{max} *versus* H-N (marked as H-N_2 for **1** and **2**; H-N_3 for others – Table S1 and Scheme 2), including compounds **2**, **6**, **7**, **8**, **9**, **10** and **12**, were obtained (Fig. S41).

Table 5 Results of the LFER correlations for *E* form of mCHs obtained using Eq. (3).

Comps.	**2–5**, **7**, **9–10**				
Solvent[a]	$\nu_0 \times 10^{-3}$, cm^{-1}	$\rho \times 10^{-3}$, cm^{-1}	R	Sd	F
EtOH	31.00 ± 0.37	4.02 ± 0.59	0.95	0.54	46.807
MeOH	31.28 ± 0.33	3.85 ± 0.53	0.96	0.48	54.076
2CE	31.26 ± 0.42	3.83 ± 0.66	0.93	0.62	33.24
H_2O	31.77 ± 0.55	4.14 ± 0.84	0.91	0.78	24.31
AcN	31.35 ± 0.42	3.91 ± 0.67	0.93	0.63	33.48
Chl	31.27 ± 0.26	3.99 ± 0.42	0.97	0.39	89.18
DMSO	30.66 ± 0.34	3.80 ± 0.61	0.94	0.57	37.95

[a] Abbreviation for the solvents are given in Table S2.

Table 6 Correlation results for the NMR data of mCHs with σ constants using Eq. (3).

	ρ	h	R	F	Sd	n	Compound included
H(N)	0.35 ± 0.04	10.39 ± 0.030	0.94	50.71	0.07	9	**1, 2, 3, 4, 5, 11, l1*, l2*, l3***
H(C═N)	0.15 ± 0.02	7.79 ± 0.02	0.933	33.53	0.038	7	**3, 4, 5, 11, l2*, l3*, l4***
C═N	0.45 ± 0.06	140.16 ± 0.04	0.964	52.09	0.092	6	**2, 3, 11, 12, 12*, l4***
C═O	−0.93 ± 0.12	157.40 ± 0.07	0.95	50.18	0.15	8	**1, 3, 4, 5, 10, 12, l1*, l4***

* Literature data are given in Table S4.

General trend reflects the importance of the molecular structure, electronic density distribution, and HBD capability of appropriate sites at studied mCHs (Papadakis et al., 2012). Presence of methyl group causes both appropriate structural adaptation and anisotropy effect, which exert significant shielding of hydrogen atom in compounds **6**–**9**, and thus leads to higher ν_{max} and lower NMR chemical shifts (Fig. S41).

A positive linear plot were obtained for inter-correlation of ν_{max} *versus* ^{13}C NMR data of azomethine carbon (C═N) chemical shifts for compounds **1**, **3**, **8**, **9**, **10** and **11** (Fig. S42). The deshielding of the carbon nuclei of the azomethine carbon is a strong indication of the electron withdrawing character of the azomethine substiteunt, and reflect state of the electronic density distribution in the arylimino conjugated part of mCHs. The compound **10** showed lower ν_{max} and higher shielding at C═N carbon as a consequence o more polarizable π-electronic density over 8-qunilonylimino moiety.

3.5. Photochromism of carbohydrazones

An interesting phenomenon related to the processes of *E*/*Z* – photoisomerization of pyridine substituted semicarbazone in solution was evidenced by the C═N double bond isomerization. The same process was previously found to be operative in (*E*)-4-phenyl-1-(pyridine-2-yl-methylene)semicarbazone which exhibits photochromism in solution and in the solid state. ^{1}H NMR chemical shifts of **N3-H** was found at lower value for 0.22 ppm upon UV irradiation, as a consequence of *cis–trans* photoizomerization, and the mechanistic pathway was confirmed using UV, 2D NOESY NMR analysis, and crystal structure study. In addition, it was shown that the isomerization rate depends on temperature and solvent used (Lin et al., 2012).

In accordance with those literature data and results from NMR and UV study in this work, and considering the higher stability of *E* form of all studied compounds in DMSO, it was of interest to investigate the factors influencing *E*/*Z* isomerization of selected compounds. As an example, ^{1}H and ^{13}C NMR analysis indicate that **3** and **7** exist in *E* form in DMSO solution, while results of theoretical calculations showed their higher stability in *Z* form due to the formation of intramolecular hydrogen bond (Table 2). Equilibria shift, i.e. *E*/*Z* isomerization, was accomplished under the influence of external stimuli such as irradiation by electromagnetic waves in the UV region. In accordance with that, upon UV illumination of *E* form of compounds **3** and **7**, they photoisomerize to *Z* isomer. Effectivness of the process depends on energetic barrier of isomerization, stability of *E* and *Z* form, and contribution of the intra-molecular hydrogen bonding to stabilization of compounds **3** and **7** in *Z* form (Fig. S28).

In order to perform a kinetic study of the *cis–trans* photoisomerization, compounds **1**–**9** were exposed to UV radiation for the appropriate time interval in the range 0–120 min. Time-dependent absorption spectra upon UV irradiation at 254 nm (or 366 nm) in DCM and MeOH showed that compounds **1**, **4**–**6** and **8** did not isomerise, while isomerisation were observed for compound **2** in MeOH and **3**, **7** and **9** in DCM. Representative UV spectra of compounds **3** and **7** in DCM, **8** and **9** in DCM and **2** in DCM and MeOH are given in Figs. 4, S43 and S44, respectively. The absorption maxima of **3**, **7** and **9** appear at 292.3 nm, 292.0 nm and 283.0 nm in DCM, respectively. Upon UV irradiation, a new band appeared at 320–400 nm and 250–280 nm in DCM with an isosbestic point observed at 323.0 and 260.0 nm for **7**, 320.0 nm for **9** and 318.0 and 260.0 nm for **3**. This is a spectral indication of the occurrence of photoisomerization in solution. These results are in accordance with TD-DFT results, *i.e.* theoretical and experimental spectra obtained before and after UV irradiation of compound **7** in *E* and *Z* form (Fig. S45).

The photoisomerization of pyridine based compounds **3**, **7** and **9** in solution under 364 nm light irradiation was found to obey the first order kinetics in DCM (Figs. 5 and S46), while for **4**, **5** and **8** no observable isomerization were detected (Fig. S43a)). According to our results and literature finding (Lin et al., 2012) it could be stated that ortho-position of the pyridine nitrogen with respect to the C═N bond leads to the most photoreactive sequence in a isomerisation process. Significance of intra-molecular bond in a stabilization of photoisomerized pyridyl and acyl hydrazones was also evidenced by results from 2D ^{1}H NMR spectroscopy (Chaur et al., 2011). In accordance to that higher stability of the *E* form of compounds **4**, **5** and **8** in DCM togehter with no additional stabilization in excited state by hydrogen bonding indicate that isomerisation is unfavorable process. Oppositely, compound **2** do not isomerize under irradiation by UV light in DCM due to the stabilizing effect of strong hydrogen bond operative in the *E* form of initial state (Fig. S27).

Lin et al. (2012) showed that isomerisation of semicarbazides based on pyridinecarbaldehydes with nitrogen in para-position is also feasible process. In our study it was found that photoisomerization of compound **9**, with para-position of pyridyl nitrogen, in DCM take place at limited extent after 120 min of illumination (Fig. S43b)). Contribution of both electronic effect of ”aza” group in para-position and steric effect of methyl group support isomerisation, but unstable excited state in *Z* form is susceptible to spontaneous reversal process to *E* form. On the contrary, photoisomerized compounds **3** and **7** in DCM even after 10 days still occupy *Z* conformation in the dark due to stabilization by hydrogen bonding.

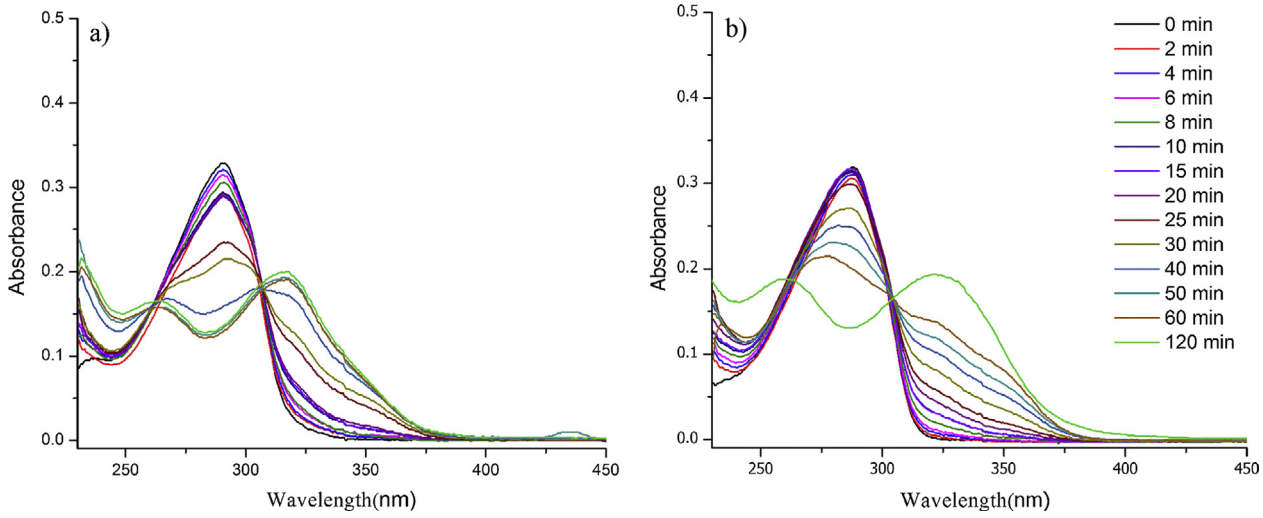

Fig. 4 Evolution of UV absortion spectra during the irradiation of **3** (a) and **7** (b) (1.0×10^{-5} mol dm^{-3}) in DCM.

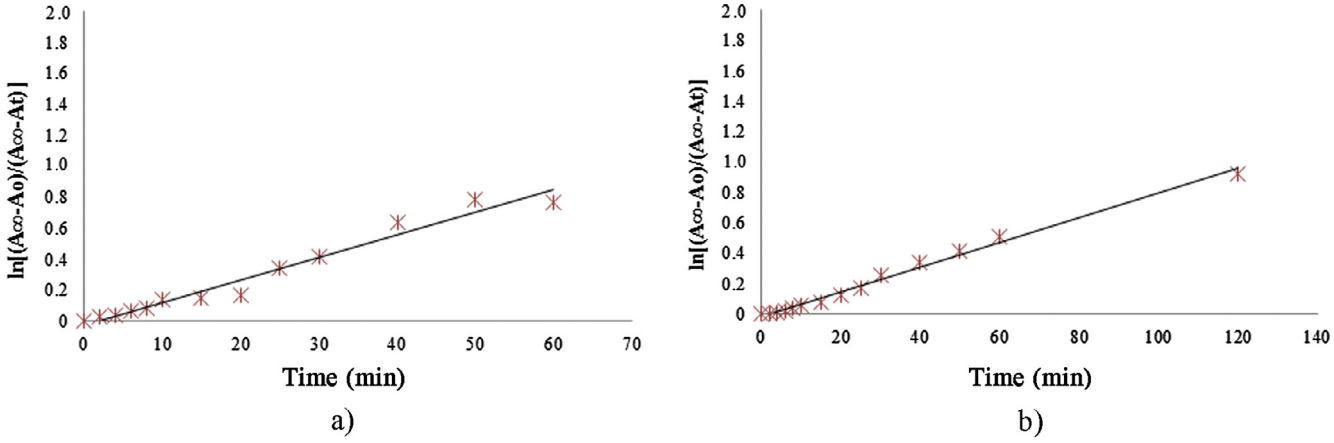

Fig. 5 Plot of $\ln[(A_\infty - A_0)/(A_\infty - A_t)]$ with time for the photoisomerization of **3** (a) and **7** (b) under 364 nm light irradiation.

Results of the photoisomerization of compound **3** and **7** under 364 nm light irradiation was processed using first order kinetic equation, by plotting $\ln[(A_\infty - A_0)/(A_\infty - A_t)]$ *versus* time where: A_0, A_∞ and A_t are the observed absorption data corresponding to 323.0 and 318.0 nm wavelength in DCM at time zero, i.e. infinite time, and time t of the isomerization process, respectively. Photoisomerization of **3** and **7** have finished after 60 and 120 min, respectively (Fig. 5). Steric repulsion of a methyl group, present at imine carbon in **7**, contribute to faster reversal isomerization to initial state than **3** under influences of daylight. These results indicate a significance of steric effect of imine methyl group to the interaction/interference with stability of the excited state of studied compounds.

The analogous isomerization experiments were performed in MeOH. The influence of MeOH on the hydrogen bonding in pseudocyclic structure of compound **2** (Fig. S27) may differ from DCM due to a contribution of solvent hydrogen bonding interaction. This effect cause destabilization of ground state of **2** by disturbing the intramolecular hydrogen bond (Fig. S27; **2**-a). This hypothesis was confirmed by very fast isomerization of **2** in MeOH, which take place in 15 min. After standing in the dark for 48 h, the *E* form is completely restored (Fig. S44).

Further photoisomerization studies have shown that irradiation of **3** and **7** in MeOH did not induce any observable change in the UV spectra. Such behavior strongly confirms the significance of hydrogen bonding established by intermolecular solvent/solute interactions, which prevail over intramolecular one created by a cyclic structure in *Z* form (Fig. S28; 3-b).

In order to evaluate effect of the intra-molecular hydrogen bonding to stabilization of *Z* form of **3** and **7** the geometries of these isomers were reoptimized in DCM and MeOH with ωB97X-D/6-311G(d,p) method. The ωB97X-D functional was used because it includes empirical dispersion and long range corrections. Recent benchmark studies have shown a very good behavior of this functional for describing geometry and energy of strong hydrogen bonds (Thanthiriwatte et al., 2011). The calculation results showed that intra-molecular hydrogen bond contribute to stabilization of Z isomer. The energies of *E* form are 1.85 and 0.68 kcal higher than of *Z* form

Table 7 Results of ωB97X-D/6-311G(d,p) and AIM calculations of **2**, **3** and **7** in DCM.

Comp.	Tautomer	Energy (kcal)	N—H (Å)	ρ	$\nabla^2\rho$	μ (D)
2	*E*	0.0	1.772	0.0445	0.119	6.5526
	Z	11.55				4.6091
3	*E*	1.85				2.4733
	Z	0.0	1.908	0.0346	0.107	7.9018
7	*E*	0.68				2.9123
	Z	0.0	1.849	0.0396	0.118	8.0533

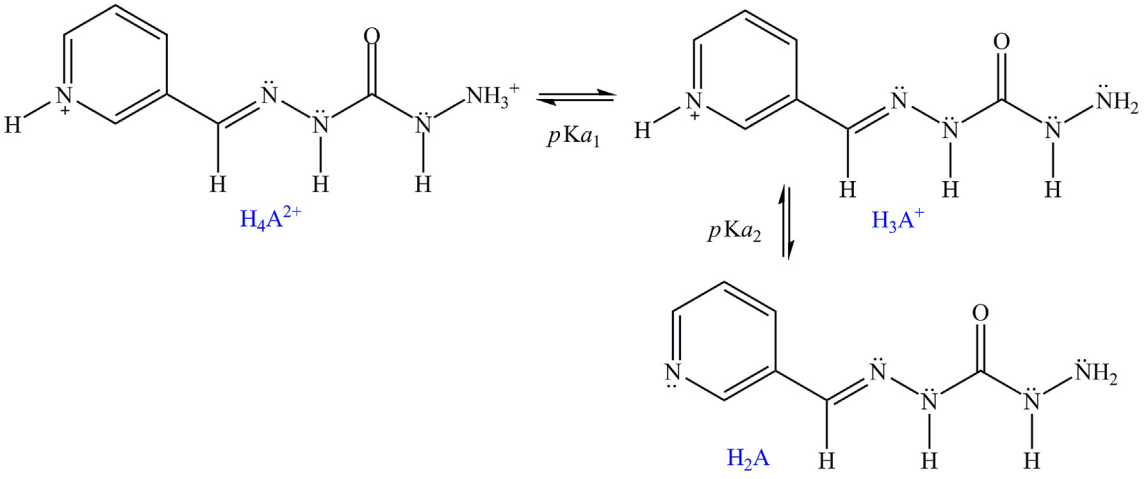

Scheme 4 Protonation states of **4**.

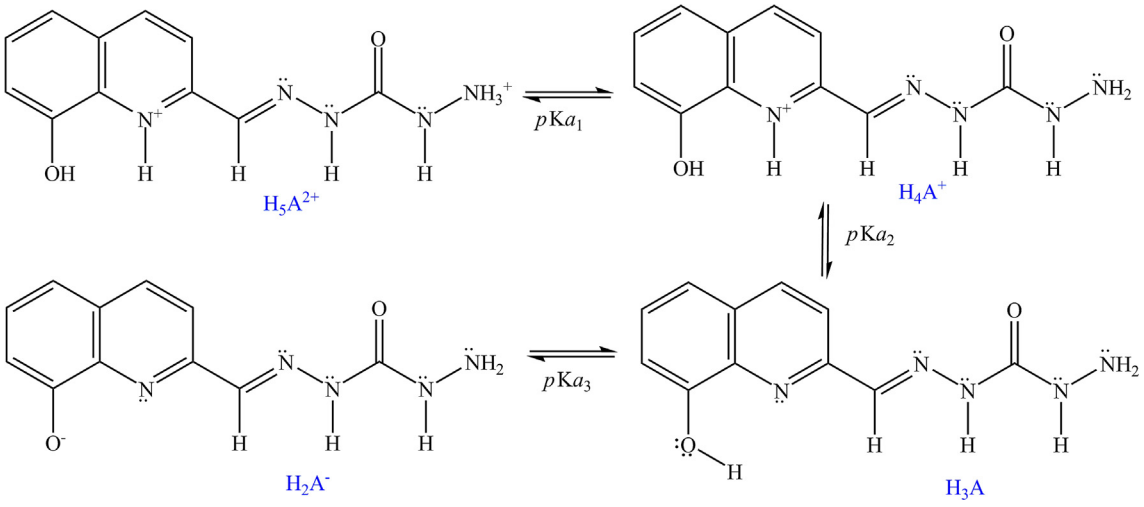

Scheme 5 Protonation states of **12**.

(Table 7). The low energy differences between isomers indicate that an intra-molecular hydrogen bond formed in *Z* form contributes to stabilization of such structure. This was further confirmed by structural and topology analysis.

The distances between nitrogen and hydrogen atoms involved in hydrogen bond creation in *Z* tautomers of **3** and **7** are 1.908 and 1.849 Å in DCM and 1.906 and 1.846 in MeOH (Tables 7 and S9), respectively. Even lower values were obtained for **2**, 1.772 (Table 7) and 1.764 Å (Table S9). These values are significantly lower then sum of corresponding van der Waals radii (2.6 Å). AIM topological analysis has found a bond critical point (BCP) between nitrogen and hydrogen atom in *Z* form of **3** and **7**. Data about found BCP's are summarized in Tables 7 and S6. Values for total electronic density (ρ) at BCP, 0.0346 to 0.0445 in DCM; Table 7, and 0.0348 to 0.0454 in MeOH (Table S9), respectively, fall at the high density range for hydrogen bond (0.002–0.035) (Thanthiriwatte et al., 2011). Since total electron density at the BCP correlates with hydrogen bond strength (Koch and Popelier, 1995; Yuan et al., 2010), higher electron density value in *E* isomer of

compound **2** further confirms a presence of stronger hydrogen bond in this compound, than in *Z* isomers of compounds **3** and **7.** Such findings are in agreement with photoisomerization data.

3.6. Acidity constants determination

Acidity constants determination was performed in order to define proton-donating/accepting capabilities of Lewis acid/basic sites in mCHs. More details is given in Supplementary material. Determination of pK_a were performed both experimentally and compared to predicted values (ADMET Predictor, 2015) to confirm successfulness of applied experimental methodology. Acidity constants were potentiometrically determined in H_2O (**1–9**) and MeOH:H_2O (**10–12**) (1:1, v:v) at $t = 25 \pm 1$ °C, and at constant ionic strength ($I = 0.1$ mol L^{-1} (NaCl)). Solutions of NaOH (0.1 mol L^{-1}) and HCl (0.1 mol L^{-1}) were prepared in deionized H_2O and MeOH:H_2O (1:1, v:v) and potentiometrically standardized. For working solution, studied compound was dissolved in MeOH and diluted with the equivalent volume of aqueous 0.2 M NaCl ($c = 0.5–1.1 \times 10^{-3}$ mol L^{-1}). Prior to titration, 100.0 µL of standard 0.1 mol L^{-1} HCl solution was added to 4.00 mL of working compound solution. All samples were

Table 8 Experimentally determined (pK_{aexp}) and calculated (pK_{acalc}) values of mCHs.

	pK_{a1exp}	pK_{a1calc}*	pK_{a2exp}	pK_{a2calc}*	pK_{a3exp}	pK_{a3calc}*
1	3.27 ± 0.05	2.79[a]				
2	3.44 ± 0.02	3.51			9.38 ± 0.05	8.94
3	2.77 ± 0.01	2.72	4.32 ± 0.01	4.16		
4	3.17 ± 0.06	2.94	4.48 ± 0.06	4.08		
5	3.29 ± 0.07	2.98	5.07 ± 0.07	4.41		
6	3.22 ± 0.06	2.76[a]				
7	2.93 ± 0.06	2.73	4.71 ± 0.05	3.93		
8	3.19 ± 0.11	2.99	4.83 ± 0.09	4.13		
9	3.28 ± 0.04	3.01	5.13 ± 0.02	4.20		
10	2.41 ± 0.21	2.82	4.08 ± 0.03	3.72		
11	2.83 ± 0.05	3.08	4.21 ± 0.11	4.33		
12	2.53 ± 0.08	2.68	4.68 ± 0.06	3.72	9.54 ± 0.11	9.03

* All predictions are based on *E* isomers of compounds **1–12** (ADMET Predictor, 2015).
[a] http://www.chemaxon.com.

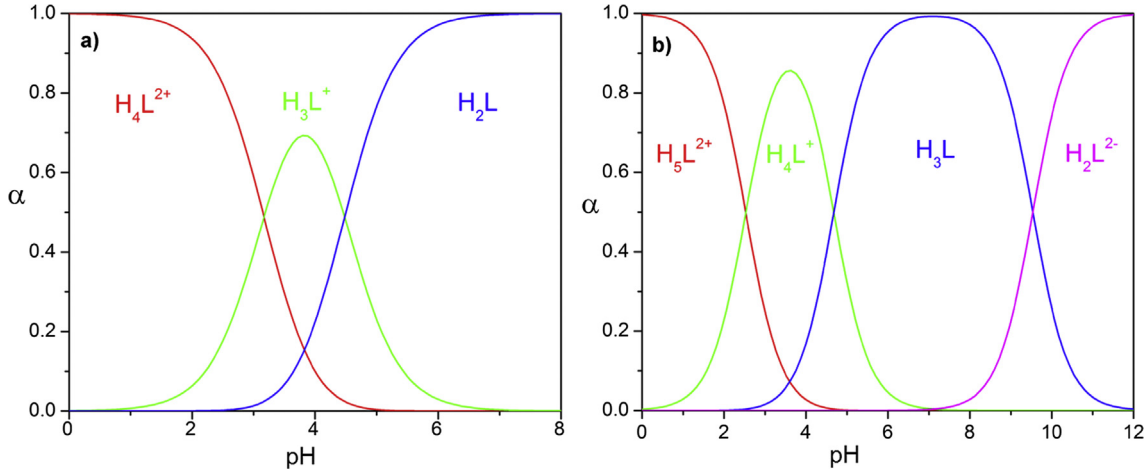

Fig. 6 Species distribution diagrams of compounds **4** and **12** (**α** = molar species fraction) calculated from experimentally determined pKa values.

Table 9 Correlation results of the pK_a values of mCHs with σ^{+}_{pH} constants (Table S4) using Hammett Eq. (3).

	ρ	h	R	F	Sd	n	Comps. included
(pK_{a1})NH_3^+	2.61 ± 0.08	0.29 ± 0.04	0.96	49.09	0.06	6	**3–5** and **7–9**
(pK_{a2})NH^+(OH)	3.80 ± 0.25	0.51 ± 0.13	0.92	16.28	0.01	6	**3–5** and **7–9**

Table 10 Results of TD-DFT calculations for transitions from ground to first vertical excited state in DMSO.

Compound/ isomer	Energy (eV)	Oscillator strenght	Excitation	CI expansion coefficient	% of single particle excitation contribution
1/*E*	4.5721	0.8329	HOMO → LUMO	0.69413	96.36
1/*Z*	4.9323	0.4692	HOMO → LUMO	0.68389	93.54
2/*E*	4.3751	0.4378	HOMO → LUMO	0.68013	92.52
			HOMO-1 → LUMO	0.12199	2.98
2/*Z*	4.8737	0.2377	HOMO → LUMO	0.65268	85.20
			HOMO-1 → LUMO	0.10068	2.03
			HOMO → LUMO + 1	0.14749	4.35
			HOMO-1 → LUMO + 2	0.13082	3.42
3/*E*	4.6647	0.8708	HOMO → LUMO	0.69183	95.73
3/*Z*	4.4597	0.5978	HOMO → LUMO	0.68932	95.03
4/*E*	4.6117	0.7878	HOMO → LUM O	0.6889	94.92
5/*E*	4.6815	0.8384	HOMO → LUMO	0.69372	96.25
6/*E*	4.7889	0.7242	HOMO → LUMO	0.69115	95.64
6/*Z*	5.2377	0.3730	HOMO → LUMO	0.68398	93.56
7/*E*	4.6999	0.7626	HOMO → LUMO	0.69092	95.47
7/*Z*	4.458	0.5501	HOMO → LUMO	0.69117	95.54
8/*E*	4.7798	0.6454	HOMO → LUMO	0.68091	92.73
8/*Z*	5.1039	0.0184	HOMO → LUMO	0.33081	21.89
			HOMO-1 → LUMO	−0.1172	2.75
			HOMO-2 → LUMO	0.30703	18.85
			HOMO-3 → LUMO	0.47447	45.02
			HOMO-5 → LUMO	0.11188	2.50
			HOMO-7 → LUMO	−0.11158	2.49
9/*E*	4.7902	0.6856	HOMO → LUMO	0.68797	94.66
9/*Z*	5.0762	0.0025	HOMO → LUMO	−0.13373	3.58
			HOMO-1 → LUMO	0.19789	7.83
			HOMO-2 → LUMO	0.54799	60.06
			HOMO-3 → LUMO	−0.3013	18.16
			HOMO-2 → LUMO + 2	0.10459	2.19
10/*E*	4.045	0.588	HOMO → LUMO	0.68888	94.91
11/*E*	4.3282	0.7059	HOMO → LUMO	0.57551	66.24
			HOMO → LUMO + 1	−0.13347	3.56
			HOMO-1 → LUMO	0.29287	17.15
			HOMO-2 → LUMO	0.1049	2.20
12/*E*	4.0394	0.3024	HOMO → LUMO	0.6808	92.70
			HOMO-1 → LUMO + 1	0.14272	4.07

titrated with 2.0 μL increments of standard 0.1 mol L^{-1} NaOH solution to obtain pH in the range 1.8–12.2. HyperQuad 2008 software (Gans and O'Sullivan, 2000) was used to calculate the acidity constant values pK_{a1} and pK_{a2} from four repeated titrations. As example, possible protolytic equilibria in solution (pH range 1.8–12.2) are shown for compounds **4** and **12** on Schemes 4 and 5, and results of pK_a determination in Table 8. Analyzed mCHs contain significant numbers of potential proton-accepting and proton-donating sites with different capabilities to release or accept proton depending on local/overall electronic density environment. In accordance with that some dissociation processes are beyond of used pH range 1.8–12.2, and thus not presented.

As an example, species distribution diagrams for **4** and **12** as a function of pH are given in Fig. 6. Experimental data show that ionization of the protonated hydrazinyl amino group showed acidic character, with low dependence on "aza" group position (comps. **3–5** and **7–9)** and steric interference of methyl group present in **7–9**. Similar pK_{a1exp} values of **10–12** with respect to **3** and **7**, reflect the main influence of electron-accepting character of substituent present at imine carbon. Small variation of the ionization constants of protonated terminal amino group is mainly influenced by the degree of the attenuation of long range transmission of substituent effect through amide bond of urea structure. On the other hand, the value of ionization constant of protonated pyridine/quinoline ring (pK_{a2}) behave in a similar/regular fashion indicating that contributing effects to changes of both pK_{a1exp} and pK_{a2exp} are similar and not significantly distance/position dependent. Electron-donating capability of hydroxy group in **12** contribute to slight increase of pK_{a1} value. As can be seen from trends in compounds **3–5**, and **7–9**, both pK_{a1} and pK_{a2} values increase as pyridyl nitrogen change position from 2 to 4. It proves the appropriate significance of electron-withdrawing effect of protonated pyridyl substituent on acidity of terminal hydrazinyl amino group.

Moreover, acidity of phenolic oxygen in both **2** and **12** are similar which menas that low influence of electronic structure and intermolecular hydrogen is operative in compound **2**. Such behavior is influenced by HBD/HBA solvent effects contributing by strong solvation diminishing effect of inter-molecular hydrogen bonding.

Due to extended conjugation through the imine group of studied mCHs it could produce the electronic density shift to

Table 11 Calculated D_{CT} and Q_{CT} values of mCHS in the course of electronic excitation.

Compound/isomer	Q_{CT} (e-)	D_{CT} (Å)
1/*E*	0.448	0.835
1/*Z*	0.543	2.130
2/*E*	0.583	1.320
2/*Z*	0.487	0.858
3/*E*	0.484	1.134
3/*Z*	0.577	2.180
4/*E*	0.497	1.465
5/*E*	0.743	2.378
6/*E*	0.443	0.907
6/*Z*	0.622	2.782
7/*E*	0.471	1.284
7/*Z*	0.614	2.482
8/*E*	0.558	2.516
8/*Z*	0.725	1.254
9/*E*	0.732	2.208
9/*Z*	0.706	1.377
10/*E*	0.421	2.629
11/*E*	0.374	0.401
12/*E*	0.614	3.183

carbohydrazide moiety affecting proton-donating/accepting properties of approrpiate sites capable for dissociation. In order to understand/quantify the influence of structural effect/ionization constants of their prospective sites at investigated molecules, *i.e.* the electronic effect of substituent present on imine carbon, LFER analysis, using SSP Eq. (3), was performed. The results of correlation of calculated pK_a values (Table 8) with selected substituent constant (Table S4) are given in Table 9 and Fig. S47.

Obtained results clearly showed that proportionality between pK_{a1} *versus* σ_{pH}^{+} showed significant influence on proton-releasing capability indicating that increased electron-accepting power of substituent at imine carbon cause lower acidity of both protonated amino and pyryidine groups.

3.7. TD-DFT calculations: nature of the frontier molecular orbitals and quantification of ICT

Changes in the overall charge distribution in both ground and excited states were studied by calculation of HOMO/LUMO energies (E_{HOMO}/E_{LUMO}) and E_{gap} values in gas phase and DMSO. Obtained results are presented in Figs. S48 and S49, and Table S10. TD-DFT results for transitions from ground to first vertical excited state in DMSO are given in Table 10. No significant ICT could be noticed from the structure of HOMO-LUMO orbitals. Generally, E_{gap} values were lower for quniolyl containing compounds. The largest energy gaps of 9.282 and 9.168 eV were found for compounds **8** and **9** in *Z* form, while the lowest energy gaps were observed for **10**–**12** with 7.610, 7.961 and 7.630 eV, respectively. This is consistent with the largest batochromic shift of their absorption maxima relative to unsubstituted compound. It can be noticed that the densities of the HOMO and LUMO orbitals for all compounds are more or less uniformly distributed over the whole molecule, indicating low extent of ICT in the course of excitation. It can also be noted that the density of the HOMO/LUMO orbitals, populated on the heterocyclic ring, due to strong electron accepting character of the nitrogen substituent causes π-electron density shift from the rest of molecule regardless to oppositely oriented, but weaker electron-accepting character of the carbohydrazide moiety.

Obviously, the ICT process is more feasible in compounds with higher π-electronic density, *i.e.* **10**–**12**, due to higher polarizability of excited state which can be, under influences of surrounding solvent environment, preferentially stabilized with respect to the ground state (Table 10). Due to this, the excited and ground states are closer and more rapid internal conversion take place. Variation of structural/substituent patterns clearly indicates that contributions of both factors: structural and substituent/compound donor–acceptor characters are involved in the ICT mechanism of the investigated molecules. Additional results from TD-DFT calculations, oscillator strengths, vertical excitation energies and electronic transitions are provided in Table 10. TD-DFT results have indicated a large contribution of single HOMO to LUMO excitations in ground to first excited state transition (greater than 90% for *E* isomer; Table 10). Only in the case of 2-quinolinyl compound **11**, there is an appropriate participation of HOMO-1 to LUMO excitation (17.15%), HOMO-2 → LUMO (2.20%) and HOMO → LUMO + 1 (3.56%). In conclusion, for all compounds calculated E_{gap} values were consistent with experimental results obtained from UV–Vis measurement.

ICT occurs when photon absorption promotes a significant deformation of the electronic cloud due to appropriate (partial/total) electronic shift from one moiety of a molecule to another. In order to quantify this phenomenon, a simple and efficient model was used for definition/evaluation of ICT on the basis of the overall charge distribution computed and changes in the in both ground and excited states (Ciofini et al., 2012; Jacquemin et al., 2012; Le Bahers et al., 2011). TD-DFT method was used for quantification of the ICT by calculations of the charge-transfer distance (D_{CT}) and amount of transferred charge (Q_{CT}).

Processes of electronic excitations takes place by a photon absorption, which cause a electron density shift from one part to another part of the molecule in the course of electronic transition. Calculated distance between two barycenters of the electronic density, D_{CT} and Q_{CT} are presented in Table 11 for both isomers. ICT processes of *E* and *Z* isomers are given on Figs. 7 and S50. It is noticeable that the strongest ICT occurs in **5** and **9**, *i.e.* 4-pyridyl substituted compounds, showing transfer of 0.743 e^- over 2.378 Å and 0.732 e^- over 2.208 Å, respectively. On the other hand, in compound **11,** with 2-quinolyl substituent, intramolecular charge transfer of only 0.374 e^- over 0.401 Å is evidently a local process within π-electronic system of substituent (Fig. 7). The variation of substituent patterns in imine side of investigated molecules indicates that contributions of both conformational arrangement and donor–accepting character are involved in the ICT mechanism of the investigated molecules (Figs. 7 and S50).

The presented experimental and theoretical study implies that the solvatochromic and physico-chemical properties of studied mCHs are the consequence of the overall effect of the molecule's geometry, influenced by the electronic substituent effects transmitted through π–conjugated systems. Results obtained in this study might help in assessing the potential application of the investigated compounds in future study.

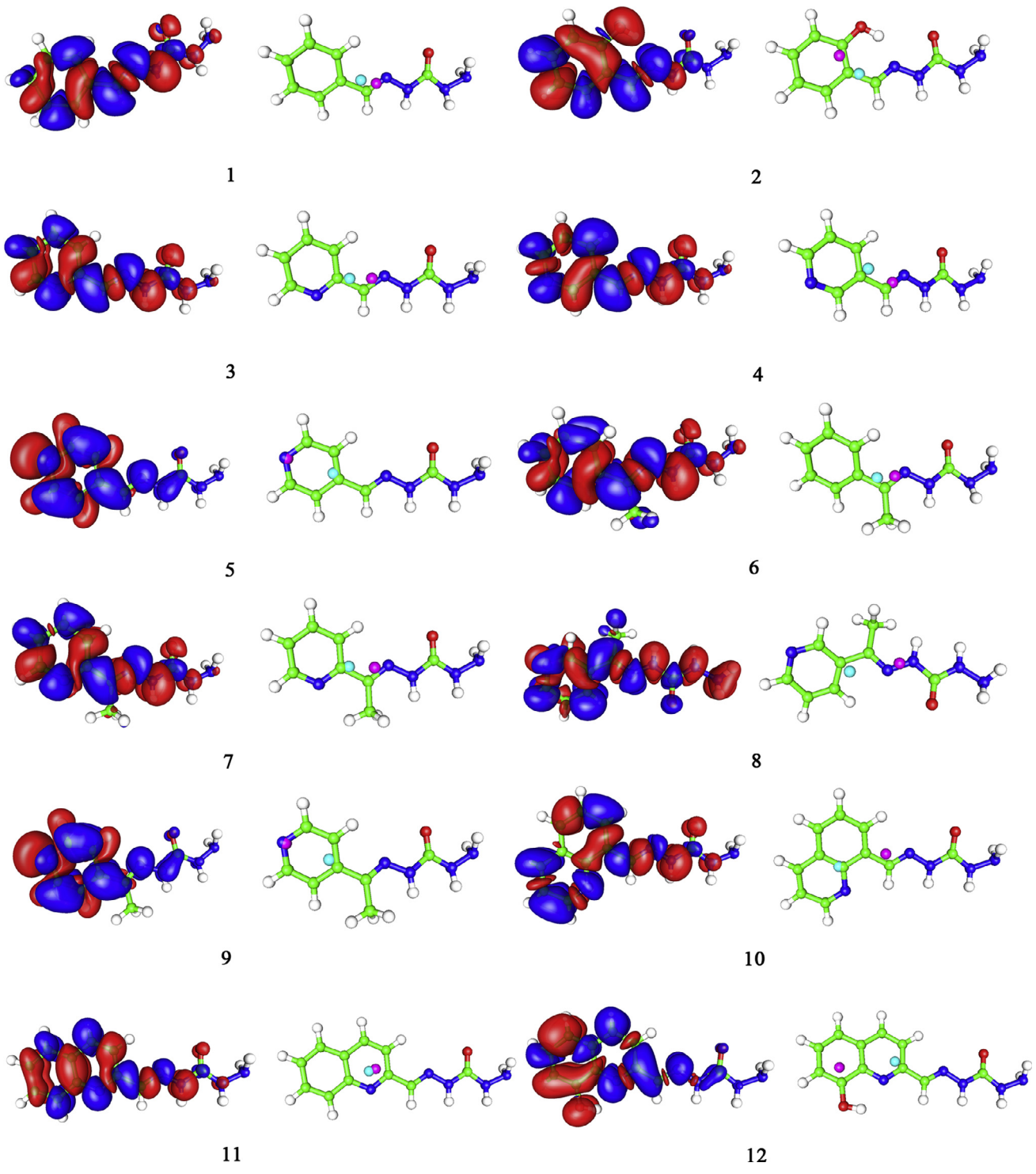

Fig. 7 ICT processes in compounds **1**–**12**, E form; Left images – difference between densities in excited and ground state (red and blue – density increase and decrease upon transition, respectively); Right images – positions of barycenters for charge loss (cyan circle) and charge gain (violet circle) upon transition.

4. Conclusions

The substituent and solvent effects on the UV–Vis absorption maxima shifts of investigated monocarbohydrazones were successfully evaluated from the experimental data and theoretical calculations. Solvent polarizability is the principal factor which generally showed influencing the shift of absorption maxima, whereas the solvent dipolarity, acidity

and basicity are of lower importance. The absorption maxima undergo a bathochromic shift with increasing solvent dipolarity/polarizability and hydrogen bond accepting capability indicating that the excitation state is more polarizable than the ground state. Specific interactions through hydrogen bond donating effect were attributed mainly to the N-H hydrogen and carbonyl oxygen, and it is slightly affected by the substituent present.

Moreover, electronic effect of substituents change the extent of conjugation, affecting the ICT process. From the crystal structure of **5** and **9**, and optimized geometries of investigated compounds, it was evident that that substituents induce a small change in torsion angles α, β, χ and δ, holding a system in almost perfectly planar geometry. Strong electron-donor, i.e. hydroxyl group, did not support significantly an electron density shift to carbonyl group. Calculation of the HOMO-LUMO energy gaps contributed to understanding the mechanism of electronic excitations. Largest energy gaps of 8.606 eV (**3**) and similar values in the range 8.292–8.558 eV for **2–5, 7** and **9** were obtained. Lowest energy gaps were found for quinoline based CHs in the range 7.610–7.961 eV, respectively, which is consistent with their largest batochromic shift. Electron density of the HOMO and LUMO orbital for all compounds showed low extent of ICT, which is mostly affected by electron-accepting character of pyridyl and quinolyl rings.

All compounds have shown an ionization equilibrium in highly acidic medium with pK_{a1} values between 2.41 and 3.44. This process was attributed to the ionization of protonated hydrazinyl amino group. Second ionization equlibirium was a dissociation of protonated nitrogen atom from pyridine/quinoline ring, with pK_{a2} values between 4.08 and 5.13. The electron withdrawing effect of pyridyl N atom was important for the first ionization process, which also confirmed the transmission of electronic effect through the whole molecule.

Introduction of methyl group of imine moiety to some extent increased both pK_a values, which can be explained with electron donating effect of Me group, as well as the slight distorsion of planar geometry which reduces a possibility for conjugate stabilization of a system.

Although calculation showed that the *E* isomers of mCHs are the most stable forms in the majority of compounds studied, irradiation with UV light may cause photoisomerization to *Z* form. Depending on the substitution pattern of compounds, and solvent polarity/hydrogen bonding ability photoisomerization may finish in 15 min, in a couple of hours, or be completely absent. Presented comprehensive experimental and theoretical study on mCHs offered a wealth valuable results useful in QSPR and future QSAR analysis.

Acknowledgements

This work was supported by the Ministry of Education, Science and Technological Development of Serbia (Project Nos. 172013 and 172055).

Appendix A. Supplementary material

Supplementary data associated with this article can be found, in the online version, at http://dx.doi.org/10.1016/j.arabjc.2017.08.010.

References

Abu El-Reash, G.M., El-Gammal, O.A., Ghazy, S.E., Radwan, A.H., 2013. Characterization and biological studies on Co(II), Ni(II) and Cu(II) complexes of carbohydrazones ending by pyridyl ring. Spectrochim. Acta – Part A Mol. Biomol. Spectrosc. 104, 26–34. http://dx.doi.org/10.1016/j.saa.2012.11.008.

Abu El-Reash, G.M., El-Gammal, O.A., Radwan, A.H., 2014. Molecular structure and biological studies on Cr(III), Mn(II) and Fe(III) complexes of heterocyclic carbohydrazone ligand. Spectrochim. Acta – Part A Mol. Biomol. Spectrosc. 121, 259–267. http://dx.doi.org/10.1016/j.saa.2013.10.048.

ADMET Predictor, 2015. version 7.2. Simulations Plus, Inc.

Al-Hazmi, G.A.A., Metwally, N.E., 2017. A series of nickel(II) complexes derived from hydrazide derivatives, electrochemical, thermal and spectral studies. Arab. J. Chem. 10, S1003–S1013. http://dx.doi.org/10.1016/j.arabjc.2013.01.002.

Alam, M., Verma, G., Shaquiquzzaman, M., Marella, A., Akhtar, M., Ali, M., 2014. A review exploring biological activities of hydrazones. J. Pharm. Bioallied Sci. 6, 69. http://dx.doi.org/10.4103/0975-7406.129170.

Bacchi, A., Bonini, A., Carcelli, M., Ferraro, F., Leporati, E., Pelizzi, C., Pelizzi, G., 1996. Chelating behaviour of methyl 2-pyridyl ketone carbono- and thiocarbonohydrazones in copper(II) and zinc (II) complexes. J. Chem. Soc. Dalt. Trans. 2699. http://dx.doi.org/10.1039/dt9960002699.

Bacchi, A., Carcelli, M., Pelagatti, P., Pelizzi, C., Pelizzi, G., Zani, F., 1999. Antimicrobial and mutagenic activity of some carbono- and thiocarbonohydrazone ligands and their copper(II), iron(II) and zinc(II) complexes. J. Inorg. Biochem. 75, 123–133. http://dx.doi.org/10.1016/S0162-0134(99)00045-8.

Beraldo, H., Nacif, W.F., West, D.X., 2001. Spectral studies of semicarbazones derived from 3- and 4-formylpyridine and 3- and 4-acetylpyridine: crystal and molecular structure of 3-formylpyridine semicarbazone. Spectrochim. Acta – Part A Mol. Biomol. Spectrosc. 57, 1847–1854. http://dx.doi.org/10.1016/S1386-1425(01)00413-9.

Božić, A., Filipović, N.R., Novaković, I., Bjelogrlić, S., Nikolic, J., Drmanic, S., Marinković, A., 2017. Synthesis, antioxidant and antimicrobial activity of carbohydrazones. J. Serbian Chem. Soc. 82, 1–14. http://dx.doi.org/10.2298/JSC161220045B.

Božić, A., Marinković, A., Bjelogrlić, S., Todorović, T.R., Cvijetić, I. N., Novaković, I., Muller, C.D., Filipović, N.R., 2016. Quinoline based mono- and bis-(thio)carbohydrazones: synthesis, anticancer activity in 2D and 3D cancer and cancer stem cell models. RSC Adv. 6, 104763–104781. http://dx.doi.org/10.1039/C6RA23940D.

Catalán, J., 2009. Toward a generalized treatment of the solvent effect based on four empirical scales: dipolarity (SdP, a New Scale), Polarizability (SP), Acidity (SA), and Basicity (SB) of the medium. J. Phys. Chem. B 113, 5951–5960. http://dx.doi.org/10.1021/jp8095727.

Chaur, M.N., Collado, D., Lehn, J.M., 2011. Configurational and constitutional information storage: multiple dynamics in systems based on pyridyl and acyl hydrazones. Chem. – A Eur. J. 17, 248–258. http://dx.doi.org/10.1002/chem.201002308.

Ciofini, I., Le Bahers, T., Adamo, C., Odobel, F., Jacquemin, D., 2012. Through-space charge transfer in rod-like molecules: lessons from theory. J. Phys. Chem. C 116, 11946–11955. http://dx.doi.org/10.1021/jp3030667.

Craik, D.J., Brownlee, R.T.C., n.d. Substituent Effects on Chemical Shifts in the Sidechains of Aromatic Systems, in: Progress in Physical Organic Chemistry. John Wiley & Sons, Inc., Hoboken, NJ, USA, pp. 1–73. http://dx.doi.org/10.1002/9780470171936.ch1.

El-Gammal, O.A., Abu El-Reash, G.M., Ghazy, S.E., Radwan, A.H., 2012. Synthesis, characterization, molecular modeling and antioxidant activity of (1E,5E)-1,5-bis(1-(pyridin-2-yl)ethylidene)carbonohydrazide (H2APC) and its zinc(II), cadmium(II) and

mercury(II) complexes. J. Mol. Struct. 1020, 6–15. http://dx.doi.org/10.1016/j.molstruc.2012.04.029.

Farrugia, L.J., 1999. WinGX suite for small-molecule single-crystal crystallography. J. Appl. Crystallogr. 32, 837–838. http://dx.doi.org/10.1107/S0021889899006020.

Farrugia, L.J., 1997. ORTEP -3 for Windows - a version of ORTEP - III with a Graphical User Interface (GUI). J. Appl. Crystallogr. 30, 565–566. http://dx.doi.org/10.1107/S0021889897003117.

Frisch, M.J., Trucks, G.W., Schlegel, H.B., Scuseria, G.E., Robb, M. A., Cheeseman, J.R., Scalmani, G., Barone, V., Mennucci, B., Petersson, G.A., Nakatsuji, H., Caricato, M., Li, X., Hratchian, H. P., Izmaylov, A.F., Bloino, J., Zheng, G., Sonnenberg, J.L., Hada, M., Ehara, M., Toyota, K., Fukuda, R., Hasegawa, J., Ishida, M., Nakajima, T., Honda, Y., Kitao, O., Nakai, H., Vreven, T., Montgomery, J.J.A., Peralta, J.E., Ogliaro, F., Bearpark, M., Heyd, J.J., Brothers, E., Kudin, K.N., Staroverov, V.N., Kobayashi, R., Normand, J., Raghavachari, K., Rendell, A., Burant, J.C., Iyengar, S.S., Tomasi, J., Cossi, M., Rega, N., Millam, J.M., Klene, M., Knox, J.E., Cross, J.B., Bakken, V., Adamo, C., Jaramillo, J., Gomperts, R., Stratmann, R.E., Yazyev, O., Austin, A.J., Cammi, R., Pomelli, C., Ochterski, J.W., Martin, R.L., Morokuma, K., Zakrzewski, V.G., Voth, G.A., Salvador, P., Dannenberg, J.J., Dapprich, S., Daniels, A.D., Farkas, O., Foresman, J.B., Ortiz, J. V., Cioslowski, J., Fox, D.J., 2009. Gaussian 09, Revision D.01.

Gans, P., O'Sullivan, B., 2000. GLEE, a new computer program for glass electrode calibration. Talanta 51, 33–37. http://dx.doi.org/10.1016/S0039-9140(99)00245-3.

Hansch, C., Leo, A., Hoekman, D., 1995. Exploring QSAR: Hydrophobic, Electronic, and Steric Constants. Explor. QSAR Hydrophobic, Electron. Steric Constants. http://dx.doi.org/10.1021/jm950902o.

Jacquemin, D., Bahers, T. Le, Adamo, C., Ciofini, I., 2012. What is the "best" atomic charge model to describe through-space charge-transfer excitations? Phys. Chem. Chem. Phys. 14, 5383. http://dx.doi.org/10.1039/c2cp40261k.

Jansma, A., Zhang, Q., Li, B., Ding, Q., Uno, T., Bursulaya, B., Liu, Y., Furet, P., Gray, N.S., Geierstanger, B.H., 2007. Verification of a designed intramolecular hydrogen bond in a drug scaffold by nuclear magnetic resonance spectroscopy. J. Med. Chem. 50, 5875–5877. http://dx.doi.org/10.1021/jm700983a.

Kamlet, M.J., Abbound, J.L.M., Taft, R.W., 1981. An examination of linear solvation energy relationships. In: Taft, R.W. (Ed.), Progress in Physical Organic Chemistry. John Wiley & Sons, New York, pp. 485–630.

Karmakar, A., Manna, B., Desai, A.V., Joarder, B., Ghosh, S.K., 2014. Dynamic metal-organic framework with anion-triggered luminescence modulation behavior. Inorg. Chem. 53, 12225–12227. http://dx.doi.org/10.1021/ic501477u.

Koch, U., Popelier, P.L.A., 1995. Characterization of C-H-O hydrogen bonds on the basis of the charge density. J. Phys. Chem. 99, 9747–9754. http://dx.doi.org/10.1021/j100024a016.

Kogan, V.A., Lukov, V.V., Novotortsev, V.M., Eremenko, I.L., Aleksandrov, G.G., 2005. Dinuclear copper (II) complexes with an unsymmetrical exchange fragment. Russ. Chem. Bull. Int. Ed. 54, 600–605.

Kothari, R., Sharma, B., 2010. Synthesis, spectroscopic characterization and invitro antimicrobial investigation of some Hg(II) complex of carbohydrazone. Orient. J. Chem. 26, 1577–1579.

Le Bahers, T., Adamo, C., Ciofini, I., 2011. A qualitative index of spatial extent in charge-transfer excitations. J. Chem. Theory Comput. 7, 2498–2506. http://dx.doi.org/10.1021/ct200308m.

Lin, L., Fan, W., Chen, S., Ma, J., Hu, W., Lin, Y., Zhang, H., Huang, R., 2012. Photochromism of (E)-4-phenyl-1-(pyridine-2-ylmethylene)semicarbazide. New J. Chem. 36, 2562. http://dx.doi.org/10.1039/c2nj40468k.

Lozan, V., Lassahn, P.-G., Zhang, C., Wu, B., Janiak, C., Rheinwald, G., Lang, H., 2003. Dinuclear nickel(II) and palladium(II) complexes in combination with different co-catalysts as highly active catalysts for the vinyl/addition polymerization of norbornene, Z. Naturforsch. B.

Lu, T., Chen, F., 2012. Multiwfn: a multifunctional wavefunction analyzer. J. Comput. Chem. 33, 580–592. http://dx.doi.org/10.1002/jcc.22885.

Manoj, E., Kurup, M.R.P., Suresh, E., 2008. Synthesis and spectral studies of bisthiocarbohydrazone and biscarbohydrazone of quinoline-2-carbaldehyde: crystal structure of bis(quinoline-2-aldehyde) thiocarbohydrazone. J. Chem. Crystallogr. 38, 157–161. http://dx.doi.org/10.1007/s10870-007-9267-9.

Novak, P., Jednačak, T., Parlov Vuković, J., Zangger, K., Rubčić, M., Galić, N., Hrenar, T., 2012. Synthesis, structural characterization and hydrogen bonding of mono(salicylidene)carbohydrazide. Croat. Chem. Acta 85, 451–456. http://dx.doi.org/10.5562/cca2123.

Okawara, T., Imai, K., Ochiai, T., 2006. Free radical scavenger containing semicarbazide derivatives. WO/2006/093124.

Oxford Diffraction CrysAlis CCD and CrysAlis Red. Oxford Diffraction, 2009.

Papadakis, R., Deligkiozi, I., Tsolomitis, A., 2012. Synthesis and characterization of a group of new medium responsive non-symmetric viologens. Chromotropism and structural effects. Dye. Pigment. 95, 478–484. http://dx.doi.org/10.1016/j.dyepig.2012.06.013.

Papadopoulos, M.G., Sadlej, A.J., Leszczynski, J. (Eds.), 2006. Non-Linear Optical Properties of Matter. Springer Netherlands, Dordrecht. http://dx.doi.org/10.1007/1-4020-4850-5.

Patel, R.N., 2010. Structural, magnetic and spectroscopic characterization of two unusual end-on bis(l-acetato/l-nitrato) bridged copper(II) complexes with N0-[phenyl(pyridin-2-yl) methylidene]-furan-2-carbohydrazide and (2E,4Z)-N,2-dimethylhepta-2,4,6-trienamide-1-phenyl-1. Inorganica Chim. Acta 363, 3838–3846. http://dx.doi.org/10.1016/j.ica.2010.07.026.

Rančić, M.P., Stojiljković, I., Milošević, M., Prlainović, N., Jovanović, M., Milčić, M.K., Marinković, A.D., 2019. Solvent and substituent effect on intramolecular charge transfer in 5-arylidene-3-substituted-2,4-thiazolidinediones: experimental and theoretical study. Arab. J. Chem. 12 (8), 5142–5161. http://dx.doi.org/10.1016/j.arabjc. 2016.12.013..

Reynolds, W.F., Gomes, A., Maron, A., MacIntyre, D.W., Tanin, A., Hamer, G.K., Peat, I.R., 1983. Substituent-induced chemical shifts in 3- and 4-substituted styrenes: definition of substituent constants and determination of mechanisms of transmission of substituent effects by iterative multiple linear regression. Can. J. Chem. 61, 2376–2384. http://dx.doi.org/10.1139/v83-412.

Rosales, D., 1985. Asymmetric derivatives of carbohydrazide and thiocarbohydrazide as analytical reagents. Talanta 32, 467–474. http://dx.doi.org/10.1016/0039-9140(85)80258-7.

Rubčić, M., Galić, N., Halasz, I., Jednačak, T., Judaš, N., Plavec, J., Šket, P., Novak, P., 2014. Multiple solid forms of 1,5-Bis(salicylidene)carbohydrazide: polymorph-modulated thermal reactivity. Cryst. Growth Des. 14, 2900–2912. http://dx.doi.org/10.1021/cg500203k.

SCALE3 ABSPACK CrysAlisPro, Agilent Technologies, Version 1.171.35.19.

Sheldrick, G.M., 2015. Crystal structure refinement with SHELXL. Acta Crystallogr. Sect. C Struct. Chem. 71, 3–8. http://dx.doi.org/10.1107/S2053229614024218.

Sutradhar, M., Barman, T.R., Rentschler, E., 2014. Coordination versatility of 1,5-bis(salicylidene)carbohydrazide in Ni(II) complexes. Inorg. Chem. Commun. 39, 140–143. http://dx.doi.org/10.1016/j.inoche.2013.11.018.

Swathy, S.S., Selwin Joseyphus, R., Nisha, V.P., Subhadrambika, N., Mohanan, K., 2016. Synthesis, spectroscopic investigation and

antimicrobial activities of some transition metal complexes of a [(2-hydroxyacetophenone)-3-isatin]-bishydrazone. Arab. J. Chem. 9, S1847–S1857. http://dx.doi.org/10.1016/j.arabjc.2012.05.004.

Taploo, C.L., Dhar, D.N., 1982. Schiff-bases and their applications. J. Sci. Ind. Res. 41, 501–506.

Thanthiriwatte, K.S., Hohenstein, E.G., Burns, L.A., Sherrill, C.D., 2011. Assessment of the performance of DFT and DFT-D methods for describing distance dependence of hydrogen-bonded interactions. J. Chem. Theory Comput. 7, 88–96. http://dx.doi.org/10.1021/ct100469b.

Wiggins, P., Williams, J.A.G., Tozer, D.J., 2009. Excited state surfaces in density functional theory: a new twist on an old problem. J. Chem. Phys. 131, 91101. http://dx.doi.org/10.1063/1.3222641.

Yanai, T., Tew, D.P., Handy, N.C., 2004. A new hybrid exchange–correlation functional using the Coulomb-attenuating method (CAM-B3LYP). Chem. Phys. Lett. 393, 51–57. http://dx.doi.org/10.1016/j.cplett.2004.06.011.

Yuan, L., Fairchild, M.J., Perkins, A.D., Tanentzapf, G., 2010. Analysis of integrin turnover in fly myotendinous junctions. J. Cell Sci. 123, 939–946. http://dx.doi.org/10.1242/jcs.063040.

Zelenin, K.N., Alekseev, V.V., Kuznetsova, O.B., Seminskaya, A.G., Yakimovich, S.L., Zerova, I.V., 1999. Carbonohydrazones and their ring-chain tautomerism. Russ. J. Org. Chem. C/C ZHURNAL Org KHIMII 35, 357–363.